AD-751 057

A STUDY OF THE DYNAMIC STRENGTH AND FRACTURE PROPERTIES OF ROCK

Ulric S. Lindholm, et al

Southwest Research Institute

Prepared for:

Advanced Research Projects Agency
Bureau of Mines

August 1972

A STUDY OF THE DYNAMIC STRENGTH AND FRACTURE PROPERTIES OF ROCK

by
U. S. Lindholm
L. M. Yeakley
A. Nagy

FINAL REPORT
Contract No. H0210036
Program Code No. 1F10
SwRI Project 02-3092

Sponsored by
Advanced Research Projects Agency
Monitored by
Bureau of Mines

August 1972

SOUTHWEST RESEARCH INSTITUTE
SAN ANTONIO HOUSTON

SOUTHWEST RESEARCH INSTITUTE
Post Office Drawer 28510, 8500 Culebra Road
San Antonio, Texas 78284

A STUDY OF THE DYNAMIC STRENGTH AND FRACTURE PROPERTIES OF ROCK

by
U. S. Lindholm
L. M. Yeakley
A. Nagy

FINAL REPORT
Contract No. H0210036
Program Code No. 1F10
SwRI Project 02-3092

Sponsored by
Advanced Research Projects Agency
Monitored by
Bureau of Mines

August 1972

Approved:

H. Norman Abramson, Technical
Vice President and Director
Department of Mechanical Sciences

ARPA Order Number: 1579
Amendment 2

Program Code Number: 1F10

Name of Contractor:
Southwest Research Institute

Effective Date of Contract:
March 5, 1971

Contract Expiration Date:
April 4, 1972

Amount of Contract: $61,131

Contract Number: H0 210036

Principal Investigator and
Phone Number:
U. S. Lindholm
512/684-5111

Project Scientist or Engineer
and Phone Number:
Same

Short Title of Work:
A Study of the Dynamic Strength
and Fracture Properties of Rock

FINAL REPORT

Sponsored by
Advanced Research Projects Agency
ARPA Order No. 1579, Amend. 2
Program Code 1F10

August 1972

This research was supported by the Advanced Research Projects Agency of the Department of Defense and was monitored by the Bureau of Mines under Contract No. H0210036.

DOCUMENT CONTROL DATA - R & D

(Security classification of title, body of abstract and indexing annotation must be entered when the overall report is classified)

1. ORIGINATING ACTIVITY (Corporate author)
Southwest Research Institute
P. O. Drawer 28510
San Antonio, Texas 78284

2a. REPORT SECURITY CLASSIFICATION
UNCLASSIFIED

2b. GROUP

3. REPORT TITLE
A Study of the Dynamic Strength and Fracture Properties of Rock

4. DESCRIPTIVE NOTES (Type of report and inclusive dates)
Final Technical Report

5. AUTHOR(S) (First name, middle initial, last name)
Ulric S. Lindholm
Lester M. Yeakley
Andrew Nagy

6. REPORT DATE
August 1972

7a. TOTAL NO. OF PAGES
55

7b. NO. OF REFS
16

8a. CONTRACT OR GRANT NO.
H0210036

b. PROJECT NO.

c. ARPA Order No. 1579, Amend. 2

d. Program Code 1F10

9a. ORIGINATOR'S REPORT NUMBER(S)
02-3092

9b. OTHER REPORT NO(S) (Any other numbers that may be assigned this report)

10. DISTRIBUTION STATEMENT
Distribution of this document is unlimited

11. SUPPLEMENTARY NOTES
Details of illustrations in this document may be better studied on microfiche

12. SPONSORING MILITARY ACTIVITY
Advanced Research Projects Agency
Department of Defense
Bureau of Mines

13. ABSTRACT For improvement of drilling and fragmentation techniques, additional data is needed on the strength properties of hard rock under generalized stress conditions, dynamic loading rates and a range in temperatures. This report describes the development of dynamic test techniques applicable to testing hard rock under relatively high confining pressures, presents the results of an extensive series of tests on Dresser basalt, and correlates the strength data obtained with a failure criterion which incorporates both temperature and strain rate. All tests were performed in uniaxial compression or extension with the radial confining pressure varied from 0 to 100,000 psi, strain rates from 10^{-4} to 10^{3} sec^{-1}, and temperature from 80 to 800°K. The testing was accomplished with hydraulic loading facilities at the lower strain rates and with a newly-developed Hopkinson pressure bar apparatus at the highest strain rates. The test results with Dresser basalt show a strong dependence of the ultimate or fracture strength on both temperature and rate of deformation. The combined temperature-rate dependence of the strength was such as to indicate that the fracture was controlled by a thermal activation process. A fracture criterion is formulated in terms of the three principal stresses, the temperature and the applied strain rate. It is shown that all the experimental data obtained correlates very well with this fracture criterion. The unconfined compressive strength was found to vary from 41,000 psi to 125,000 psi over the range in temperature and strain rate used in this study, with the higher strengths being obtained at low temperatures and high strain rates.

DD FORM 1 NOV 65 1473

14. KEY WORDS	LINK A		LINK B		LINK C	
	ROLE	WT	ROLE	WT	ROLE	WT
Rock Mechanics						
Strain-Rate Effects						
Fracture						
Temperature Effects						

SUMMARY

For improvement of drilling and fragmentation techniques, additional data is needed on the strength properties of hard rock under generalized stress conditions, dynamic loading rates and a range in temperatures. This report describes the development of dynamic test techniques applicable to testing hard rock under relatively high confining pressures, presents the results of an extensive series of tests on Dresser basalt, and correlates the strength data obtained with a failure criterion which incorporates both temperature and strain rate.

All tests were performed in uniaxial compression or extension with the radial confining pressure varied from 0 to 100,000 psi, strain rates from 10^{-4} to 10^{3} sec^{-1}, and temperatures from 80 to 800°K. The testing was accomplished with hydraulic loading facilities at the lower strain rates and with a newly-developed Hopkinson pressure bar apparatus at the highest strain rates. All tests at other than ambient temperature were conducted without confining pressure.

The test results with Dresser basalt show a strong dependence of the ultimate or fracture strength on both temperature and rate of deformation. The combined temperature-rate dependence of the strength was such as to indicate that the fracture was controlled by a thermal activation process. This leads to formulation of a fracture criterion of the form

$$\frac{\sigma_1}{S_C(0)} + \frac{S_C(0) - S_{BC}(0)}{S_C(0)\, S_{BC}(0)}\, \sigma_2 - \frac{\sigma_3}{S_T(0)} = 1 - \beta T\,(A - \log \dot{\epsilon}_a)$$

where σ_1 , σ_2 and σ_3 are the principal stresses, T is the test temperature and $\dot{\epsilon}_a$ is the strain rate. The constants $S_C(0)$, $S_T(0)$ and $S_{BC}(0)$ are suitably determined strength values at zero absolute temperature and β and A are constants involving the activation energy, volume and frequency. All of the experimental data obtained correlates very well with this fracture criterion. The unconfined compressive strength was found to vary from 41,000 psi to 125,000 psi over the range in temperature and strain rate used in this study, with the higher strengths being obtained at low temperatures and high strain rates. The energy required to fracture basalt in compression is also the greatest at low temperatures and at high strain rates.

TABLE OF CONTENTS

FIGURE CAPTIONS

INTRODUCTION

In order to improve drilling or other excavation techniques for hard rock, both quantitative data and physical understanding of the factors controlling the strength and fracture behavior of the rock are needed. Modern rapid excavation techniques, such as high speed rotary and percussion drilling or explosive and thermal energy deposition, produce transient mechanical and thermal loadings. Therefore, it is doubtful that static strength or fracture criteria, which involve specification only of the generalized state of stress, will be sufficient to describe these dynamic processes. We must begin to develop a kinetic theory for deformation and fracture of rock which incorporates, in addition to the state of stress, an explicit dependence on additional parameters involving time and temperature. The influence of time and temperature on the long-term response of geologic materials as in creep or stress relaxation is well appreciated. Only recently has preliminary experimental data from dynamic tests on these materials been developed. Results from these tests indicate that significant differences from static strength values may occur for short duration tests where the rate of deformation or loading is commensurate with rapid excavation techniques. The time scale of interest during impact or explosive loading of hard rock may be of the order of microseconds or even less. For tunneling machines using cutting action to grind or break away rock the shear deformation under the cutter head may occur in the order of milliseconds. Thus, rock properties over a wide range of deformation rate are required.

The importance of a wide temperature range may be less apparent. Moderate temperature variations may arise from deformation and frictional dissipation during the excavation process itself. External supply of the thermal energy to the rock mass, either in conjunction with drilling or independently, is under study as a technique for disaggregating rock. For these applications, strength properties from ambient up to the melting point may be of interest. Furthermore, in developing a kinetic theory for rock deformation and fracture, it will be shown that it is useful to vary both the deformation rate and the temperature. The rate or velocity at which most processes occur is controlled by both the elastic energy supplied by the applied stresses and the available thermal energy as measured by the temperature of the system. Thus, a systematic variation of the temperature, rate of deformation, and applied stress state, can lead to an improved understanding and qualitative description of the controlling mechanisms. This is an approach that has proved useful in the study of metals and polymers and, based upon the present results, will aid in the understanding of deformation and fracture processes in hard rock.

This report describes work initiated with two objectives in mind. First was the development of experimental techniques and generation of data using a representative type of hard rock to establish the effect of dynamic loading, temperature and state of stress on deformation and fracture properties of laboratory specimens. The second objective was the development of an appropriate and meaningful constitutive relation for the type of rock studied. A starting hypothesis for this development was the established theory for rate processes controlled by thermal activation.

The rock selected for this study was Dresser basalt obtained from a quarry in Wisconsin. All tests were performed in uniaxial compression or extension from an initial state of hydrostatic loading. Temperature and strain rate were controlled test parameters. ranging from $80^{o}K$ to $800^{o}K$ and 10^{-4} to 10^{3} sec^{-1}, respectively. The confining hydrostatic pressure was varied from 0 to 100,000 psi. The experimental techniques used and the results obtained will be described in the following sections. It will be shown that it is possible to correlate all of the data for ultimate or fracture strength with a single equation relating the stresses at fracture and the nominal deformation rate and temperature. However, it should be pointed out that, while we are able to derive quantitative estimates of such parameters as activation energies or volume, these values are only empirically derived. Our initial approach is entirely pragmatic. We have, as yet, no definition of what the rate-controlling mechanism relative to fracture may be. The relevant mechanism(s) is certainly associated with micro-crack nucleation, growth and coalescence although the role of dislocation type slip processes cannot be altogether discarded. Another potentially important control mechanism, which is not specifically included in this study, is the role of environmental corrosive effects particularly as they may influence crack growth rate. Further study of the Dresser basalt is continuing in an attempt to better define the rate-controlling mechanisms for inelastic deformation and fracture.

LITERATURE REVIEW

The vast majority of work related to determining the strength properties of rock consists of isothermal tests at what may be considered "static" testing rates. These tests are concerned with defining the elastic properties, the limit of elastic behavior (yield criterion), the inelastic flow behavior, and the limiting stress condition for fracture (fracture criterion). A fracture criterion in terms of the stress state is generally only meaningful for brittle materials which do not undergo appreciable inelastic straining. A very good general review of macroscopic criteria for flow and fracture of both ductile and brittle materials is given by Paul[1]. Paul points out the lack of experimental data on time and temperature dependent effects on flow and fracture criteria.

Cheatham[2] has reviewed work related to the effects of pressure, temperature and loading rate on mechanical properties of rocks up to about 1967. Specific mention should be made of the early work of Heard[3] with temperature and confining pressure and of Serdengecti and Boozer[4] with strain rate and temperature. The latter authors demonstrated an equivalence between the effects of strain rate, $\dot{\epsilon}$, and temperature, T, on the ultimate strength of rock specimens by employing the Zener-Holoman parameter to correlate their data. This parameter has the form

$$Z = \dot{\epsilon} \exp\left(\frac{Q}{RT}\right)$$

where Q is an activation energy and R is the gas constant. This parameter was initially proposed for describing the ductile flow of metals in tension.

More recent work has measured rock properties at loading rates such that the ultimate strength is achieved in a time scale of the order of 10 microseconds. These rates can be associated with those occurring in many rapid excavation processes. The general technique used at these high rates is the Hopkinson pressure bar. A general review of this and other high strain-rate techniques has been given by Lindholm[5].

Kumar[6] has studied the effect of stress rate and temperature on the unconfined compressive strength of basalt and granite. From this data, Kumar used the Arrhenius equation

$$\dot{\epsilon} = f \exp\left(-\frac{U(\sigma)}{RT}\right)$$

to derive a value for the stress-dependent activation energy, $U(\sigma)$, of 450 cal/mole for basalt at 50 ksi. He postulates that the strain rate sensitivity of the fracture stress is a result of the stress dependence of both the propagation velocity, V_c, of microcracks and the number of microcracks N, such that

$$\dot{\epsilon} = K \cdot N(\sigma) \cdot C \cdot V_c(\sigma)$$

where K and C are related to the orientation and average length of the microcracks. However, this appears to be more of a flow criteria than a fracture criteria.

Additional work at high strain rates has been reported by Green and Perkins[7], Perkins, Green and Friedman[8] and Brown, Swanson and Wawersik[9]. The present tests are intended to provide a more comprehensive

set of data than these preceding studies, including very wide ranges of strain rate, temperature and pressure. This will allow more definite specification of the dependence of strength on strain rate and temperature in hard rock.

EXPERIMENTAL PROCEDURES

Rock Description and Preparation

All specimens were obtained from a single boulder of Dresser basalt obtained directly from the quarry in Wisconsin. The rock is a very hard, mottled black to grey and dull olive green, very fine grained (mostly 20 to 500 micron intergrown crystals), metamorphosed (serpentinized) igneous rock with some larger serpentinized pyroxene crystals distributed throughout. Serpentinization is most thorough in an interconnecting, vein-like network throughout the rock.

Petrographic sections show the rock to be composed of a fine-grained (aphanitic) intergrown ground mass (matrix) of pyroxene, serpentine, plagioclase feldspars (mainly labradorite, bytownite, and andesine), melilite, magnetite, and a little olivine--some with a trace of iddingsite.

An intertwining network of vein-like serpentinized (metamorphosed) material is common throughout the rock. The serpentine network outlines some rounded masses (up to 1/4-inch) of rather uniformly sized intergrowths of pyroxene and feldspar containing some melilite. Magnetite and/or ilmenite occurs disseminated on the outer fringes of these ovoidal areas, as well as rather well disseminated throughout the rock. Some larger (up to 1/4-inch) crystals (phenocrysts) of partially serpentinized pyroxene occur scattered throughout. The rock can be classed as a serpentinized basalt.

Approximate mineral type, percentage composition, and crystal sizes are shown below:

Mineral	Volume	Most Crystals	Largest Crystal
Serpentine	45-60%	20-80μ	1000μ
Pyroxene	20-25	20-800	4000
Plagioclase feldspar	10-20	20 to 40 - 100 to 240	60 to 480
Magnetite &/or ilmenite	3-5	20-150	900
Melilite	3-5	80-120	320
Olivine	1	50-200	500
Iddingsite	Tr	20-100	200

The test specimens were nominally 1/2-inch in diameter and 1-inch long. They were obtained by core drilling and grinding of the ends to obtain flatness and parallelism within 0.0002 inch. Specimens were taken from three orthogonal directions in the boulder. Tests with these specimens showed that the rock was macroscopically isotropic with respect to its strength properties. Therefore, subsequent development of a fracture criterion is based upon isotropic theory.

Low and Intermediate Rate Tests

Controlled strain rate tests were performed at 1.9×10^{-4} sec^{-1} and 2.4×10^{-1} sec^{-1} with a servo-controlled hydraulic ram supplying the axial load. For tests with radial confining pressure, the chamber pressure was held constant with a servo-controlled intensifier.

The specimen arrangement is shown in Figure 1 prior to insertion into the pressure cylinder. The specimen was sealed with a thin, heat-shrinkable, polyoelfin tubing. This tubing allowed attachment of the two

clip-type extensometers shown in the figure. These extensometers employed strain-gaged flexure arms as the sensing elements. The four attachment points for each extensometer referenced directly to the rock surface through the polyoelfin tubing and were sealed with a "gage-coat" normally used to seal strain gages. The two extensometers measured radial (diametral) and axial strain continuously. Strain gages for load measurement were in series with the specimen and within the pressurized chamber. These strain gage devices are sensitive to the chamber pressure so as to produce an increasing zero shift with increasing pressure. The magnitude of the zero shift may be determined and is easily corrected for.

Chamber pressure was measured by either an external diaphragm-type pressure transducer or a piezo-resistive coil of manganin wire located inside the pressure chamber (not shown in Figure 1). Either of these transducers could be used for the pressure feedback signal.

Tests at other than room temperature were performed without confining pressure. For the low temperature tests, the loading anvils adjacent to the specimen were cooled with liquid nitrogen and the specimen brought to thermal equilibrium by conduction. For the high temperature tests the specimen and anvils were heated by radiation from quartz lamps. Temperature control was within $\pm 4^{\circ}C$. with feedback from a thermocouple mounted directly on the specimen.

Examples of the load-deformation behavior at confining pressures of 20,000 psi and 100,000 psi are shown in Figures 2 and 3. The loading path in all tests reported was initially hydrostatic with the axial stress,* σ_z, increased in proportion to the confining pressure, p. The confining pressure was then held constant at the values indicated and the axial load was either increased or decreased. The recorded stresses and strains were differential with respect to the initial hydrostatic state. For each test, two direct recordings are shown; axial stress versus strain and radial strain versus axial strain. The test at 20,000 psi (Figure 2) was carried to failure with the post-failure region after maximum load being controlled by radial strain feedback. Gross failure of the rock generally occurred at the maximum load accompanied by an audible "pop". In some cases, the strain control prevented a large stress drop but generally the failure was brittle and accompanied by a rather sudden energy release. After fracture at maximum load there was multiple faulting and the strain was no longer homogeneous. Therefore, after maximum load was reached the curves were not very reproducible.

The test of Figure 3 at 100,000 psi was reversed before the maximum stress was reached. The unloading, therefore, is largely elastic although of significantly different slope than the initial elastic modulus of 13×10^6 psi, as shown. There was also some irrecoverable strain after unloading. The apparent elastic Poisson's ratio is indicated on each figure. Derivation from elastic behavior is generally taken as the onset of dilatancy in brittle materials.

---

* Throughout this report compressive stresses and strains are taken as positive in sign as this is the dominant mode of loading.

High Rate Tests

High strain rate tests at approximately 1000 sec^{-1} were performed with a split Hopkinson pressure bar apparatus. This test technique was initially developed for the testing of metals and has been described in detail by Lindholm[10]. As mentioned previously, it has found limited use in the testing of rocks. However, there are certain limitations of the technique when applied to the testing of brittle materials.

The Hopkinson bar system is shown schematically in Figure 4. This system was modified considerably from our previous system[10] in order to allow for higher impact velocities, axial preloading, and radial confining pressure required in the testing of rock. The higher impact velocities and stresses were achieved by using a pneumatically-driven projectile (impacting bar) guided by a long launch tube. Maximum impact velocities were of the order of 2000 in./sec, limited by the maximum yield stress in the pressure bars. These bars were made from maraging steel tempered to a yield stress of approximately 350,000 psi.

The axial preload was generated by the hydraulic actuator at the far end of the transmitter pressure bar. The axial load generated by this actuator was servo-controlled in proportion to the amplitude of the radial confining pressure to produce the initial hydrostatic loading of the specimen. The axial load was reacted by an axial restraint plug having a conical collar and located at the impact end of the incident pressure bar. The impact was transmitted through this plug.

The 100 ksi pressure vessel surrounded the specimen with the pressure bars entering through packing seals at each end of the vessel. The recording strain gages on the pressure bars were outside the pressure vessel and therefore operated at ambient pressure. The pressure vessel was supported on rails and translated axially to allow access to the specimen. An overall view of the facility is shown in Figure 5 with the gas gun in the foreground.

A test with confining pressure consisted of initially applying a static hydrostatic loading by increase of the axial load from the hydraulic actuator and the pressure in the specimen chamber. These loads were then held constant and the transient axial load was applied by firing the gas gun. The strain pulses in the incident and transmitter pressure bars produced by the projectile impact were recorded on an oscilloscope. For tests at other than ambient temperature the pressure vessel was removed and heating or cooling of the specimen was achieved in a similar manner as in the static tests. The modulus variation in the pressure bars due to temperature gradients produced was not sufficient to require correction to the strain recordings in the data reduction procedure.

An example of the strain records from the pressure bars is given in Figure 6. This record is reduced in Figure 7 where the separate pulses are shifted on the time axis to account for transit time in the pressure bars. First it is noted that after the specimen fractures, denoted by the maximum

in the transmitted pulse signal, the load supported by the specimen drops to zero and the incident pulse becomes totally reflected (as at a free end). The transmitted pulse is a measure of the interface stress, σ_2 at the back end of the specimen, i.e.,

$$\sigma_2 = E_o \epsilon_T = \sigma_T$$

The interface stress, σ_1 at the front face of the specimen is

$$\sigma_1 = E_o (\epsilon_I + \epsilon_R) = \sigma_I + \sigma_R$$

where ϵ_I , ϵ_R and ϵ_T are the strain amplitude of the incident, reflected and transmitted pulses of Figure 6, and E_o is the modulus of the pressure bars.

It is seen from Figure 7 that the same maximum stress is reached at the front and back face of the specimen although there is a small time lag between the maxima. This time lag is of the order of magnitude of the wave transit time across the specimen length. We have taken this maximum stress which occurs at both faces of the specimen as the ultimate or fracture strength of the rock. This is the usual[6, 7, 8] interpretation of the split Hopkinson bar measurement. However, in this case the time to fracture is very short (approximately 10 μsec) and it is apparent from the records that stress equilibrium across the specimen is not achieved in this time interval. Therefore, inertial forces may appreciably influence the magnitude of the transient peak stress recorded. The average particle acceleration at the two faces of the specimen is of the order of 10^5 g's. If we assume the total

mass of the specimen is given this acceleration, an equivalent inertial stress of approximately 10,000 psi is produced. Thus, the true fracture stress may be overestimated by this amount. On the other hand, fracturing will tend to attenuate the amplitude of the propagating pulse as considered by Hakalehto[11]. For these reasons, there is a degree of uncertainty in the interpretation of fracture stress data for brittle materials using the Hopkinson bar or other transient pulse techniques.

The average strain rate for the dynamic tests was taken as

$$\dot{\epsilon} = \frac{\sigma_{max}}{E t_f}$$

where E is the elastic modulus of the rock and t_f is the measured time to failure. There was very little indicated inelastic deformation at these strain rates.

DEVELOPMENT OF A FRACTURE CRITERION

Before presenting the experimental results, we would like to develop the fracture criterion to which the data is compared. This will be done in essentially an empirical manner by combining terms derived from the Arrhenius rate equation to account for the temperature and strain rate effect with a static yield criterion in terms of the three principal stresses. The result is a relatively simple equation which will be shown to fit the experimental data over the entire range of parameters surprisingly well.

In its simplest form, the rate equation may be written as

$$\dot{\epsilon} = \dot{\epsilon}_o \exp - \frac{U(\sigma)}{RT} \qquad (1)$$

where the activation energy $U(\sigma)$ is assumed to be a function of the effective stress only. For the brittle rock considered here, fracture is preceded by very little inelastic strain so that it is justified to neglect inelastic strain in the formulation. The other terms in Eq. (1) are the absolute temperature T, gas constant R, and an arbitrary constant $\dot{\epsilon}_o$. When applying Eq. (1) to the fracture strength, we may consider it in the sense that

$$\dot{\epsilon} = \frac{\epsilon_f}{t_f} = \dot{\epsilon}_o \exp\left(-\frac{U(\sigma_f)}{RT}\right) \qquad (2)$$

where σ_f and ϵ_f are the stress and strain at fracture and t_f is the time required to produce fracture. This form is identical to that used by Zhurkov[12] to correlate stress-rupture data for a wide variety of materials including

metals, polymers and glasses. However, in the stress-rupture experiment a constant stress is imposed and the time to failure (or creep rate) is measured. In the present tests a constant strain rate is imposed and the resulting stress at failure is measured. Because of the difference in stress history leading to failure, there may not be an equivalence of the constants in the correlation equation used. Zhurkov found that the activation energy derived from the stress-rupture experiments was nearly equal to the heat of sublimation for many of the materials tested. Based on this observation, he suggested that the actual rupture of interatomic bonds is the controlling mechanism in kinetic fracture of solids.

The experimental data suggests that the stress dependence of the activation energy is linear and of the form

$$U(\sigma) = U_o - v\,(\sigma - \sigma_o) \qquad (3)$$

where U_o is the total activation energy of the process, v is a coefficient with dimensions of volume (often called "activation volume"), σ is the applied stress and σ_o is a constant. $(\sigma - \sigma_o)$ is the effective stress relative to the thermal activation energy. The need for inclusion of σ_o will become evident when examining the data. The linear form of Eq. (3) is not essential but is determined from the experimental data itself. Eq. (3) could be considered as a two-term truncation of a general Taylor's series expansion of $U(\sigma)$.

Substituting Eq. (3) in Eq. (1) and solving for the applied stress σ yields

$$\sigma = \frac{U_o}{v} + \sigma_o - \frac{RT}{v} \ln \frac{\dot{\epsilon}_o}{\dot{\epsilon}} \qquad (4)$$

It will be noted that $U_o/v + \sigma_o$ is the limiting stress when $T = 0$ or when $\dot{\epsilon} = \dot{\epsilon}_o$. According to Eq. (4) the applied stress at fracture will decrease linerarly with temperature and increase linearly with the logarithm of the imposed strain rate. Thus we have a relationship between temperature, strain rate and stress. The next step is to generalize this for a triaxial stress state.

Lindholm[13] has derived a generalized form of Eq. (4) in terms of the deviatoric stress and strain-rate invarients which is suitable for incremental plastic flow of ductile metals. In the present case, only a limit surface in stress space is desired which defines those combinations of the principal stress components which produce fracture. Since stress occurs only to the first order in Eq. (4), it is expedient to use a static fracture criteria which is also of first order in the stresses. The most general first order criterion is

$$A\sigma_1 + B\sigma_2 + C\sigma_3 = 1 \qquad (5)$$

where $\sigma_1 \geq \sigma_2 \geq \sigma_3$ are the three principal stresses and A, B, C are arbitrary constants. This fracture criterion has been discussed extensively

by Paul[1]. It defines a hexagonal pyramid symmetric about the hydrostatic axis and with its apex at a point of triaxial tension. If B = 0, Eq. (5) reduces to a Coulomb-Mohr criterion, and if B = 0 and C = −A it reduces to the Tresca maximum shear stress criterion. However, it has generally been shown necessary to include the intermediate principal stress ($B \neq 0$) in the fracture criterion[14, 15].

By selected tests, the three constants A, B and C may be determined. For confined compression testing it is convenient to use the fracture strengths in uniaxial compression, S_C, uniaxial tension, S_T, and biaxial compression S_{BC} so that Eq. (5) can be written

$$\frac{\sigma_1}{S_C} + \frac{S_C - S_{BC}}{S_C S_{BC}} \sigma_2 - \frac{\sigma_3}{S_T} = 1 \qquad (6)$$

However, the material strengths are all dependent upon the strain rate and temperature in accordance with Eq. (4). Here, we will have to assume that all the fracture strengths are changed in equal proportion for a given change in either temperature or strain rate. This means that the expansion or contraction of the fracture surface with change in temperature or strain rate is isotropic and a series of nesting surfaces is formed. This assumption is, of course, subject to experimental verification. We may now combine Eq. (4) and Eq. (6) to form the general fracture criterion:

$$\frac{\sigma_1}{S_C(0)} + \frac{S_C(0) - S_{BC}(0)}{S_C(0)\, S_{BC}(0)} \sigma_2 - \frac{\sigma_3}{S_T(0)} = 1 - \beta T (A - \log \dot{\epsilon}_a) \qquad (7)$$

where $\beta = \dfrac{R}{U_o + v\sigma_o}$

and $A = \log \dot{\epsilon}_o$

Also, $S_C(0)$, $S_T(0)$ and $S_{BC}(0)$ are the respective fracture strengths determined at zero absolute temperature. Experimentally these strength values are determined from extrapolation of data obtained at a number of finite temperatures.

In the final fracture criteria, we have taken $\dot{\epsilon}_a$ as some averaged or effective strain rate. At present we will side-step the issue and not say how the average should be formed, since there seems to be no meaningful guidelines. In the present tests, a dynamic load was only applied in the axial direction, so we have chosen the axial strain rate to use in the correlations. This would correspond to the maximum normal strain rate. Use of a maximum shear strain rate or one of the invarients of the strain-rate tensor would result, for the present data, only in modifying the derived constant A in Eq. (7).

The constants β and A in Eq. (7) can be determined from uniaxial compression tests ($\sigma_2 = \sigma_3 = 0$) at different temperatures and strain rates. For this the following derivatives are useful:

$$\left.\frac{d\sigma_1}{dT}\right|_{\dot{\epsilon}_a} = -\beta S_C(0)\ (A - \log \dot{\epsilon}_a) \qquad (8)$$

$$\left.\frac{d\sigma_1}{d \log \dot{\epsilon}_a}\right|_{T} = \beta T\ S_C(0) \qquad (9)$$

EXPERIMENTAL RESULTS

Stress-Strain Behavior

Some representative stress-strain curves have already been given in Figures 2 and 3. Additional curves are given in Figure 8 indicating the effects of temperature and of pressure. The curves are drawn to maximum stress only. The deformation after maximum stress was significant only with confining pressure and was not very reproducible. For the unconfined tests under all conditions there was an immediate collapse of the load to zero after maximum stress was reached.

Beginning at zero stress, there was always a distinct linear region of the stress-strain curve. The deviation from linearity or proportional limit (P.L.) is marked on the curves. For the unconfined tests there was very little deviation from linear elastic behavior before fracture at any strain-rate. Even with large confining pressure, the inelastic strain at maximum stress was of the same order of magnitude as the elastic strain.

Data for 64 tests will be presented. The principal results and values for the test parameters are summarized in Table I. The results are also plotted in the following sections and compared with Eq. (7).

Temperature and Rate Effect

The axial fracture strength in compression, S_C, is plotted as a function of temperature in Figure 9 for the three widely differing strain rates used. The solid lines are based upon Eq. (7) with the following

TABLE I. SUMMARY OF EXPERIMENTAL DATA

SP. No.	Strain Rate (Sec^{-1})	Pressure (ksi)	Temp. (^oK)	$T^*=T\log\frac{\dot{\epsilon}_o}{\dot{\epsilon}}$ (^oK)	P.L. (ksi)	Ultimate Strength (ksi)	Energy to Fracture ($in.-lb/in.^3$)
3	1.9×10^{-4}	0	300	2498	17.3	49.0	129
4	"	20	300	2498	28.0	95.0	550
5	"	10	300	2498	24.5	68.0	334
6	"	0	300	2498	16.0	58.0	167
7	"	10	300	2498	25.5	70.0	288
8	"	20	300	2498	27.5	98.5	465
9	"	20	300	2498	24.0	92.0	400
10	"	20	300	2498	29.0	102	850
12	"	10	300	2498	28.5	86.5	474
13	"	0	300	2498	32.0	49.0	230
14	"	50	300	2498	30.0	148	1550
15	"	50	300	2498	27.0	156	1690
16	"	75	300	2498	-	201	3500
23	"	0	300	2498	-	52.0	104
24	"	0	300	2498	-	56.0	112
26	2.4×10^{-1}	0	300	1567	86.0	86.0	264
38	1.9×10^{-4}	0	500	4163	37.0	43.0	69
39	"	0	500	4163	35.0	39.0	57
40	"	0	600	4995	36.0	38.0	54
41	"	0	600	4995	34.5	38.0	54
42	"	0	400	3330	37.0	42.0	66
43	"	0	500	4163	40.0	44.0	73
44	"	0	400	3300	35.0	35.5	47
45	"	0	813	6769	43.0	43.0	69
46	"	0	800	6660	-	36.8	51
47	"	0	700	5828	41.0	44.0	73
48	"	0	210	1748	60.0	78.0	237
49	"	0	198	1648	62.0	76.0	216
50	"	0	162	1349	70.0	86.5	279
51	"	0	83	691	96.0	102	388
53	2.4×10^{-1}	0	300	1567	82.0	82.0	251
54	"	0	80	418	115	115	493
55	"	0	500	2612	49.0	49.0	89
56	"	0	400	2090	-	65.5	160
57	"	0	600	3134	-	49.0	89
58	"	0	700	3657	-	46.5	81
60	"	0	800	4179	-	39.0	57
61	"	0	600	3134	-	41.0	63
63	670	0	300	533	-	112	468
66	650	0	300	530	-	109	443

SP.No.	Strain Rate (Sec^{-1})	Pressure (ksi)	Temp. (°K)	$T^* = T \log \frac{\dot{\epsilon}_o}{\dot{\epsilon}}$ (°K)	P.L. (ksi)	Ultimate Strength (ksi)	Energy to Fracture ($in.-lb/in.^3$)
67	950	0	80	130	-	126	592
68	1000	0	80	128	-	133	660
71	875	0	500	831	-	98.0	358
72	870	0	700	1165	-	103	399
74	870	0	800	1331	-	106	419
76	880	0	600	996	-	97.5	355
77	890	0	700	1158	-	85.0	270
78	880	0	800	1328	-	94.0	330
79	880	0	400	664	-	98.0	358
83	1090	10	300	470	-	120	631
85	880	0	800	1328	-	89.0	296
88	1.9×10^{-4}	75	300	2498	41	162	2020
89	"	100	300	2498	44	-	-
91	"	75	300	2498	48	179	2100
92	"	75	300	2498	48	154	1180
93	2.4×10^{-1}	10	300	1567	-	106	-
94	"	20	300	1567	106	124	-
95	"	30	300	1567	73	131	-
97	"	40	300	1567	-	169	-
98	"	50	300	1567	-	190	-
99	-1.9×10^{-4}	100	300	2498	-42	-91	-
100	-1.9×10^{-4}	85	300	2498	-38	-79	-
101	-1.9×10^{-4}	75	300	2498	-34	-74	
102	700	20	300	538	-	146	795

constants derived from the experimental data shown:

$S_C(0)$ = 125,000 psi

β = $2.21 \times 10^{-4}\ ^oK^{-1}$

A = 4.6046 ($\dot{\epsilon}_o = 4.02 \times 10^4\ sec^{-1}$)

The experimental data shows that for all temperatures a minimum stress, σ_o , is required to produce fracture. Also a maximum stress for fracture, $S_C(0)$ is achieved at T = 0. Therefore the fracture stress in compression is bounded by $\sigma_o \leq S_c \leq S_c(0)$.

A plot of compression strength versus strain rate would appear as in Figure 10, using the same constants in Eq. (7). Since the experimental data are the same as for Figure 9, only two temperatures are plotted. The strength is again bounded by σ_o and $S_C(0)$ with $\dot{\epsilon}_o$ being the limiting strain rate at which strength becomes independent of temperature. The value of $\dot{\epsilon}_o = 4.02 \times 10^4\ sec^{-1}$ is surprisingly low. An equivalent value for plastic flow in metals is 10^{10} to $10^{12}\ sec^{-1}$. From stress-rupture experiments on materials such as silver chloride, aluminum and plexiglass, Zhurkov[12] claims the order of magnitude of this parameter to be $10^{13}\ sec^{-1}$ and interprets it to be the frequency of thermal oscillations of atoms. From a similar analysis, Heard[16] obtains the value of $1.6 \times 10^7\ sec^{-1}$ from strain rate and temperature data for Yule marble. Strain rates in excess of $10^4\ sec^{-1}$ are certainly achieved in the near field of an explosive detcnation in rock. The present analysis will certainly break down in this region.

The strain rate sensitivity for fracture is seen to be large at high temperatures and high strain rates.

Figure 11 shows the effect of confining pressure on the strain rate sensitivity at 300°K. The slope of each curve is the same for all pressures in accordance with Eqs. (7) and (9).

Pressure Effect

The general effect of pressure on strength is shown in Figure 12. The experimental data is plotted on the plane passing through the axial stress, σ_z , axis and bisecting the σ_R-σ_θ plane. This plane contains the hydrostatic axis ($\sigma_z = \sigma_R = \sigma_\theta = p$). The intersection of the fracture surface with this plane is used to determine the remaining constants in Eq. (7). These are

$$S_T(0) = 46,870 \text{ psi}$$

$$S_{BC}(0) = 156,250 \text{ psi}$$

These zero temperature values are determined from the intercepts of the fracture loci, with the $-\sigma_z$ axis which gives $S_T(300) = 21,000$ psi and with the positive pressure axis which gives $\sqrt{2}\, S_{BC}(300) = 99,000$ psi.

Also shown in Figure 12 are the experimental stresses at the proportional limit or when the inelastic strain $\epsilon_p = 0$. The general loci of points where the inelastic strain equals 0.1% and 0.2% is given to indicate the extent of inelastic deformation prior to fracture. The stress at constant values of inelastic strain is much less sensitive to the hydrostatic pressure than is the fracture strength. The proportional limit surface is only slightly expanding with increasing hydrostatic pressure.

Figure 13 shows the effect of strain rate on the compression strength in the pressure plane. The fracture strength data in both Figures 12 and 13 again show the adequacy of Eq. (7) in describing the fracture criterion.

It is common to plot limit surfaces in two other planes. These are the deviatoric or π plane which is normal to the hydrostatic axis and in the biaxial planes (coordinate planes). The predicted shape of the fracture surface at T = 0 in these two planes is shown in Figure 14a and b. Due to the condition of isotropy, there is threefold symmetry in the deviatoric plane and all the biaxial coordinate planes are identical.

Energy to Fracture

For the unconfined tests (p = 0), the energy to fracture is well defined since there is no load carrying capacity after the maximum stress is reached. This energy has been calculated and is plotted in Figure 15 as a function of effective temperature T*, where

$$T^* = T \log \frac{\dot{\epsilon}_o}{\dot{\epsilon}} = T\,(A - \log \dot{\epsilon}). \qquad (11)$$

The origin of T* from Eq. (7) is apparent. It expresses the equivalence between temperature and strain rate. Similar to the fracture strength, the energy input required to fracture the basalt in compression increases with decreasing temperature and increasing strain rate. This is a result of the rock being essentially elastic to failure, therefore the energy is directly

proportional to the strength. For materials which undergo significant inelastic deformation, the energy to failure is proportional to the product of the strength and the inelastic strain to failure (ductility). Temperature and strain rate can have a large effect on ductility, e.g., the ductile to brittle transition which occurs for many metals at low temperatures. For these materials, ductility is usually reduced by decreasing temperatures and increasing strain rate. Thus, for initially ductile materials, decreasing temperature and increasing strain rate can lead to sharp reductions in energy to failure, quite the opposite of the case for basalt.

Fracture Modes

It is interesting to classify the failed rock specimens not only in terms of the test parameters but also in terms of the mode of failure. While it is realized that certain features of the fracture mode may be artifacts resulting from constraints imposed by the testing system, there were consistent changes in fracture mode with temperature, strain rate and pressure. At the same time, the system constraints on the specimen remained essentially constant.

The failures fell into four groups, namely; shear, tensile, cataclasis, and cataclasis/cleavage. An example for each of these modes is shown in Figure 16. The relationship between these failure modes and the test conditions is shown in Figure 17. Figure 17a illustrates the effect of confining pressure. A gradual transition from cataclastic cleavage, to

shear, to cataclasis is manifested as the triaxial compressive state becomes more intense, irrespective of strain rate. For unconfined uniaxial compression tests, the predominant failure mode was cataclastic cleavage. The range of shear-type failures is in general agreement with that reported previously by Serdengecti and Boozer [4] for Pala gabbro deformed at $10^{-3}\ \text{sec}^{-1} \leq \epsilon \leq 10^{1}\ \text{sec}^{-1}$. The extension tests result in a pure tensile failure.

The effect of temperature upon failure mode can be seen in Figure 17b. As the temperature decreases, a transition from apparent cataclasis to cataclasis/cleavage, a more brittle variant of cataclasis occurs just above room temperature. This behavior lends some support to the possibility of plastic flow preceding or accompanying internal microcracking. It is not otherwise obvious how a reduction in temperature is capable of affecting the development of a strictly brittle Griffith-type network of internal microcracks.

DISCUSSION OF RESULTS

The experimental results presented in the preceding section show surprisingtly good agreement for the entire range in pressure, temperature, and strain rate encompassed with the fracture criterion

$$\frac{\sigma_1}{S_C(0)} + \frac{S_C(0) - S_{BC}(0)}{S_C(0)\, S_{BC}(0)}\,\sigma_2 - \frac{\sigma_3}{S_T(0)} = 1 - \beta T (A - \log \dot{\epsilon}_a) \qquad (7)$$

The constants in this equation determined from the experimental data are:

$S_C(0)$ = 125,000 psi

$S_T(0)$ = 46,870 psi

$S_{BC}(0)$ = 156,250 psi

β = $2.21 \times 10^{-4}\ ^{o}K^{-1}$

A = 4.6046

Several features of the data and of the associated fracture criterion are worthy of note.

1. Depending upon the temperature and rate of deformation, the fracture strength will lie within a bounded region in stress space. The surface bounding the maximum strength is obtained by letting T = 0. In this case fracture must be accomplished entirely by the work done by the applied stresses as there is no thermal energy available in the system to assist in the fracture process. A similar condition occurs when the strain rate approaches the limiting rate, $\dot{\epsilon}_o$. In this case there is insufficient time available for thermal activation of the fracture process. The experimental

data also indicate that there is a lower or inner bound for the stress required to produce fracture. This is evidenced by the stress $\sigma_o = 41,000$ psi obtained in uniaxial compression. We can only conjecture that there exists an inner bounding surface in the generalized stress space. Determination of such a surface will require elevated temperature testing under triaxial stress conditions.

2. The effect of temperature and strain rate on the fracture surface is isotropic, i.e., the coefficients of the stress terms in the fracture criterion are independent of these variables. Thus, only the size of the limit surface is affected by temperature and strain rate and not its shape. While this appears true for the present tests it may not be a generally valid conclusion. We may expect that, in general, the shear and the dilational components of the stress may respond differently to temperature or to deformation rate.

3. From the data of Figure 9 and the use of Eq. (4), the apparent activation energy for fracture, U_o, may be calculated. This energy is found to be 2,600 cal/mole. Similarly, the activation volume, v, is 3.15×10^{-23} cm^3. The physical meaning of these values is uncertain at present until we can better define the rate-controlling mechanism.

4. Retaining only linear stress terms in the fracture criterion is not essential although it does retain a certain mathematical simplicity. Physically we would expect the limit surfaces to be smooth rather than

piecewise linear. From the present tests it is not possible to determine the form required for higher order stress terms. This will require additional biaxial or triaxial stress tests. From Figure 12a, it is seen that the limit surface cannot be a surface of revolution about the hydrostatic axis. Thus, it may be necessary to employ cubic terms for an adequate representation. Quadratic expressions, such as the deviatoric stress invariant, have constant amplitude in the deviatoric plane.

Future work will attempt to develop a more complete description of the fracture surface by the inclusion of biaxial tests and tests in the tensile quadrants. Studies will also be incorporated to determine the mechanisms contributing to both inelastic behavior and to failure.

REFERENCES

1. B. Paul, "Macroscopic Criteria for Plastic Flow and Brittle Fracture" in Fracture, H. Liebowitz, ed., Vol. II, Ch. 4, p. 313, Academic Press, N.Y., 1968.

2. J. B. Cheatham, "The Effect of Pressure, Temperature and Loading Rate on the Mechanical Properties of Rocks," in Mechanical Behavior of Materials Under Dynamic Loads, U. S. Lindholm, ed., Springer Verlag N.Y., p. 388, 1968.

3. H. C. Heard, "Transition from Brittle to Ductile Flow in Solenhofen Limestone as a Function of Temperature, Confining Pressure and Interstitial Fluid Pressure," Rock Deformation, Geol. Soc. Amer. Mem. 79, 193, 1960.

4. S. Serdengecti and G. D. Boozer, "The Effects of Strain Rate and Temperature on the Behavior of Rocks Subjected to Triaxial Compression," Proc. 4th Symp. Rock Mech., Penn. State Univ., 83, 1961.

5. U. S. Lindholm, "High Strain-Rate Tests," Techniques in Metals Research, Vol. 5, edited by R. Bunshah, Interscience, New York, 1971.

6. A Kumar, "The Effect of Stress Rate and Temperature on the Strength of Basalt and Granite," Geophysics, 33, 501, 1968.

7. S. J. Green and R. D. Perkins, "Uniaxial Compression Tests at Strain Rates From 10^{-4}/sec to 10^{4}/sec on Three Geological Materials," Proc. Tenth Symp. on Rock Mechanics, May 1968.

8. R. D. Perkins, S. J. Green and M. Friedman, "Uniaxial Stress Behavior of Porphyritic Tonalite at Strain Rates to 10^{3}/Second," Int. J. Rock Mech. Min. Sci., 7, 527, 1970.

9. W. S. Brown, S. R. Swanson and W. R. Wawersik, "Influence of Dynamic Loading, Biaxial Loading, and Pre-Fracturing on the Stress-Strain and Fracture Characteristics of Rocks," Final Report, DASA-2713, Univ. Utah, 1971.

10. U. S. Lindholm and L. M. Yeakley, "High Strain-Rate Testing: Tension and Compression," Jour. of Experimental Mechs, 8, 1, pp. 1-9, January 1968.

11. K. O. Hakalehto, "Brittle Fracture of Rocks Under Impulse Loads," Int. J. Fracture Mech., 6, p. 249, 1970.

12. S. N. Zhurkov, "Kinetic Concept of the Strength of Solids," Int. J. Fracture Mechanics, 1, 311, 1965.

13. U. S. Lindholm, "Some Experiments in Dynamic Plasticity Under Combined Stress," Proc., Symp. on the Mechanical Behavior of Materials Under Dynamic Loads, pp. 75-95, Springer-Verlag New York, Inc., 1968.

14. J. Handin, H. C. Heard and J. N. Magourik, "Effects of the Intermediate Principle Stress on the Failure of Limestone, Dolomite and Glass at Different Temperatures and Strain Rates," J. Geophys. Res., 72, 2, 1967.

15. K. Mogi, "Effect of Intermediate Principle Stress on Rock Failure," J. Geophys.Res., 72, p. 5117, 1967.

16. H. C. Heard, "Effect of Large Changes of Strain Rate in the Experimental Deformation of Rock," J. Geophys., 71, p. 501, 1963.

ILLUSTRATIONS

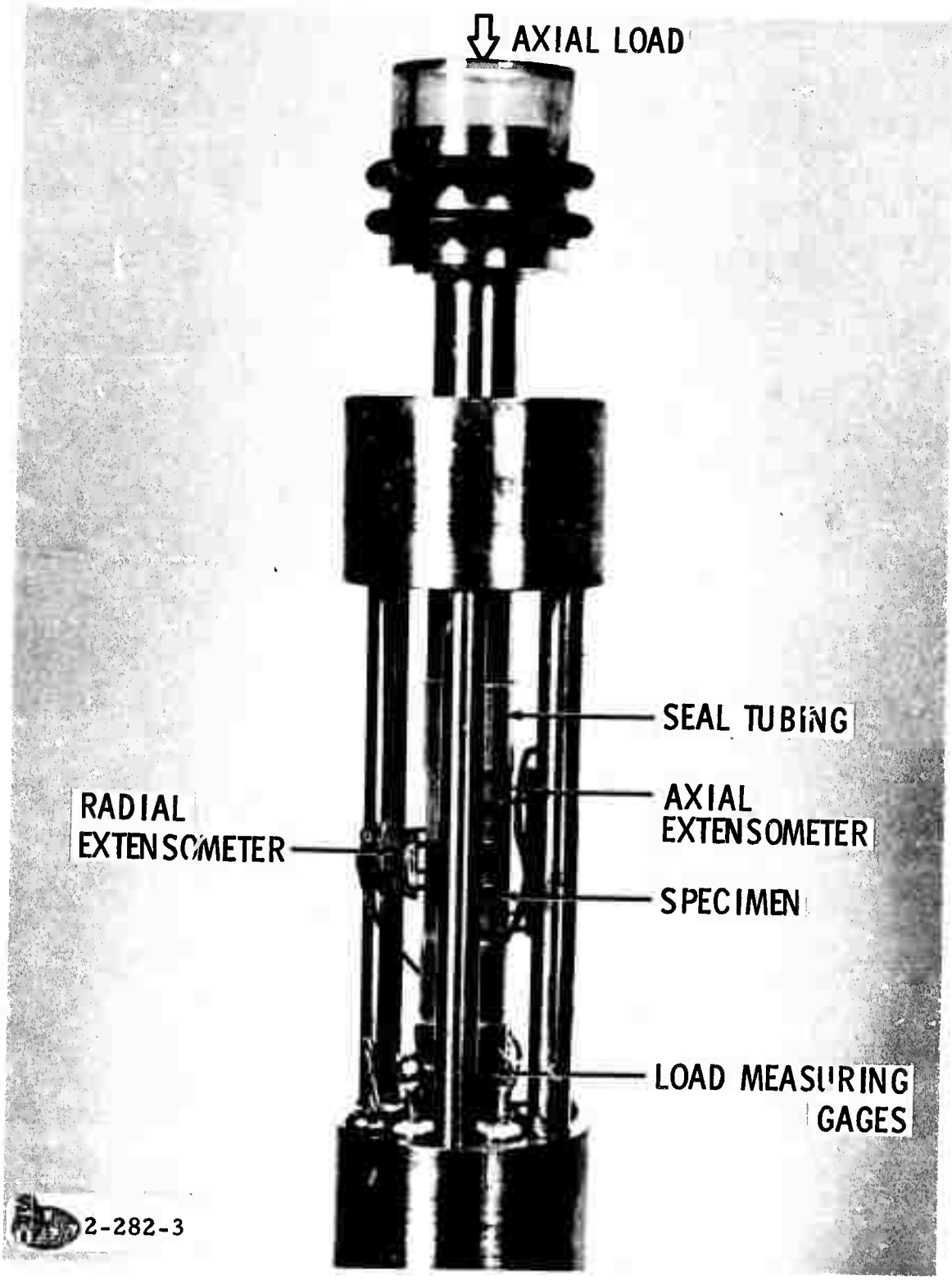

FIGURE 1. SPECIMEN ARRANGEMENT FOR LOW RATE TESTS

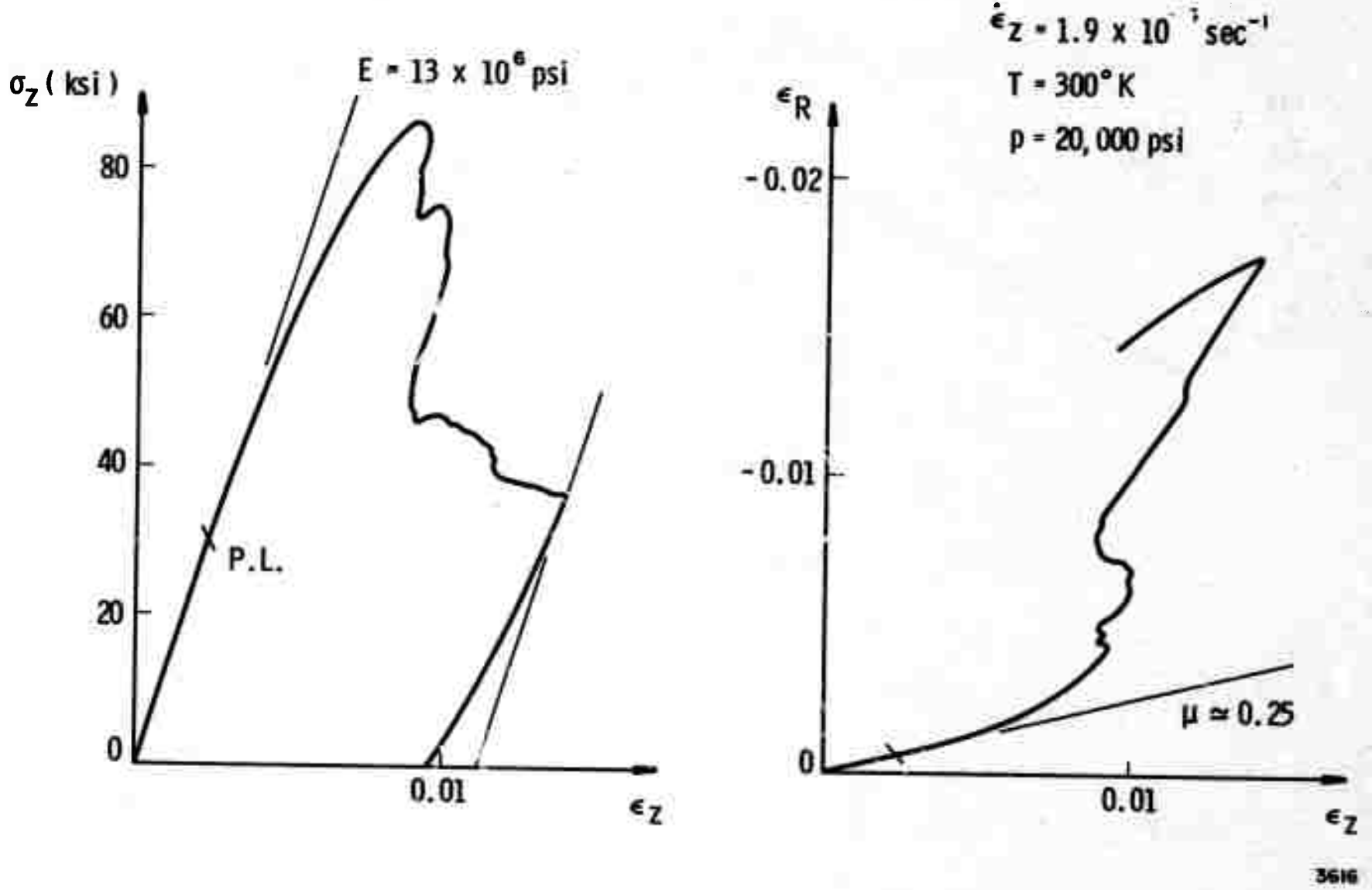

FIGURE 2. RECORD FROM LOW RATE TEST AT CONFINING PRESSURE OF 20,000 PSI

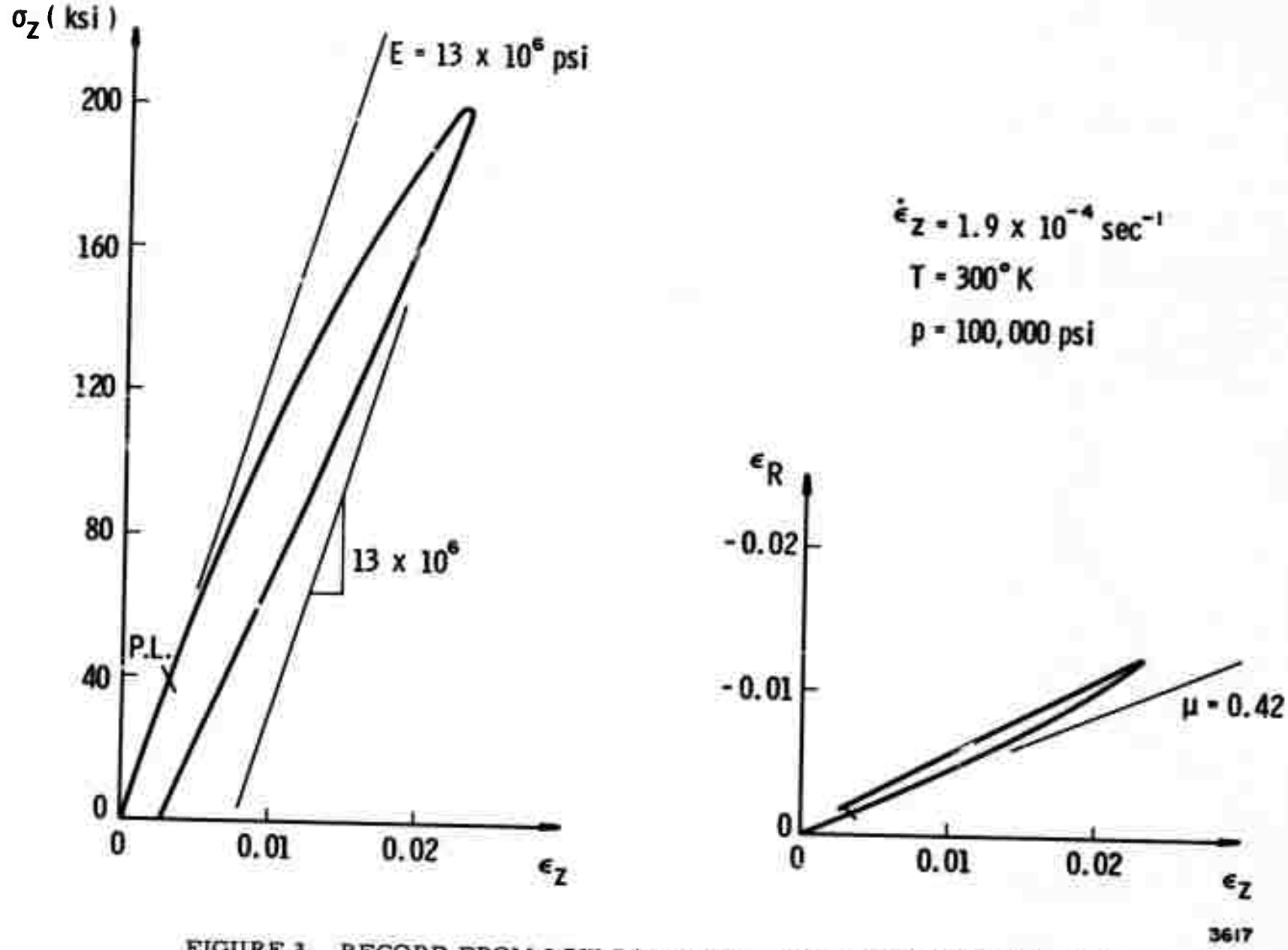

FIGURE 3. RECORD FROM LOW RATE TEST AT CONFINING PRESSURE OF 100,000 PSI

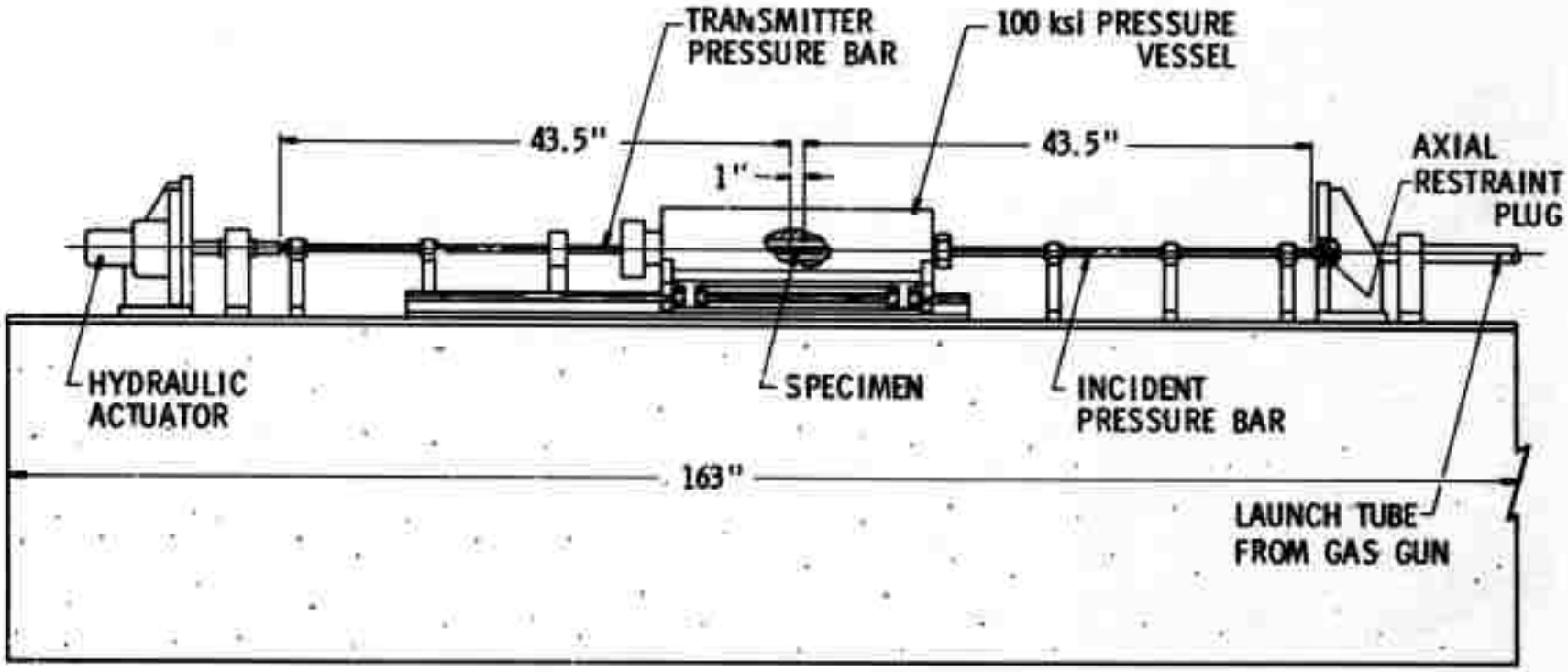

FIGURE 4. SCHEMATIC OF HOPKINSON BAR APPARATUS

3618

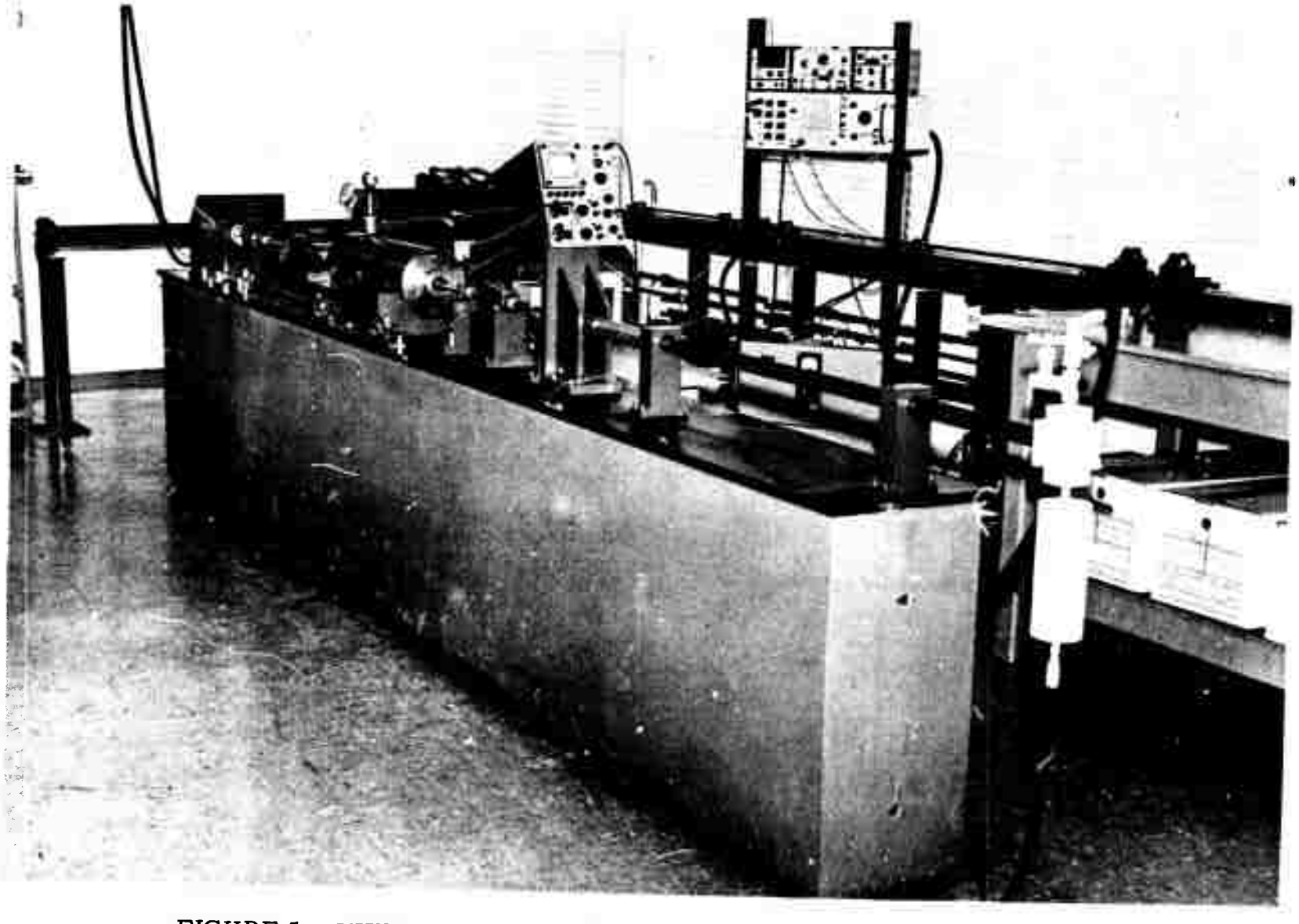

FIGURE 5. VIEW OF HOPKINSON PRESSURE BAR SHOWING GAS GUN IN FOREGROUND

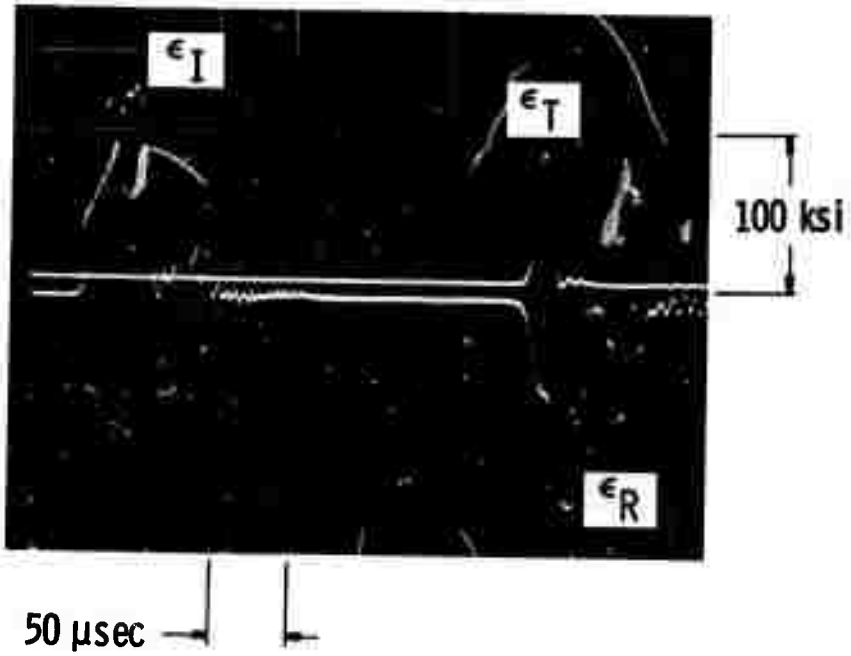

FIGURE 6. OSCILLOSCOPE TRACE OF PULSES FROM HOPKINSON BAR ($T = 300^{\circ}K$, $p = 0$)

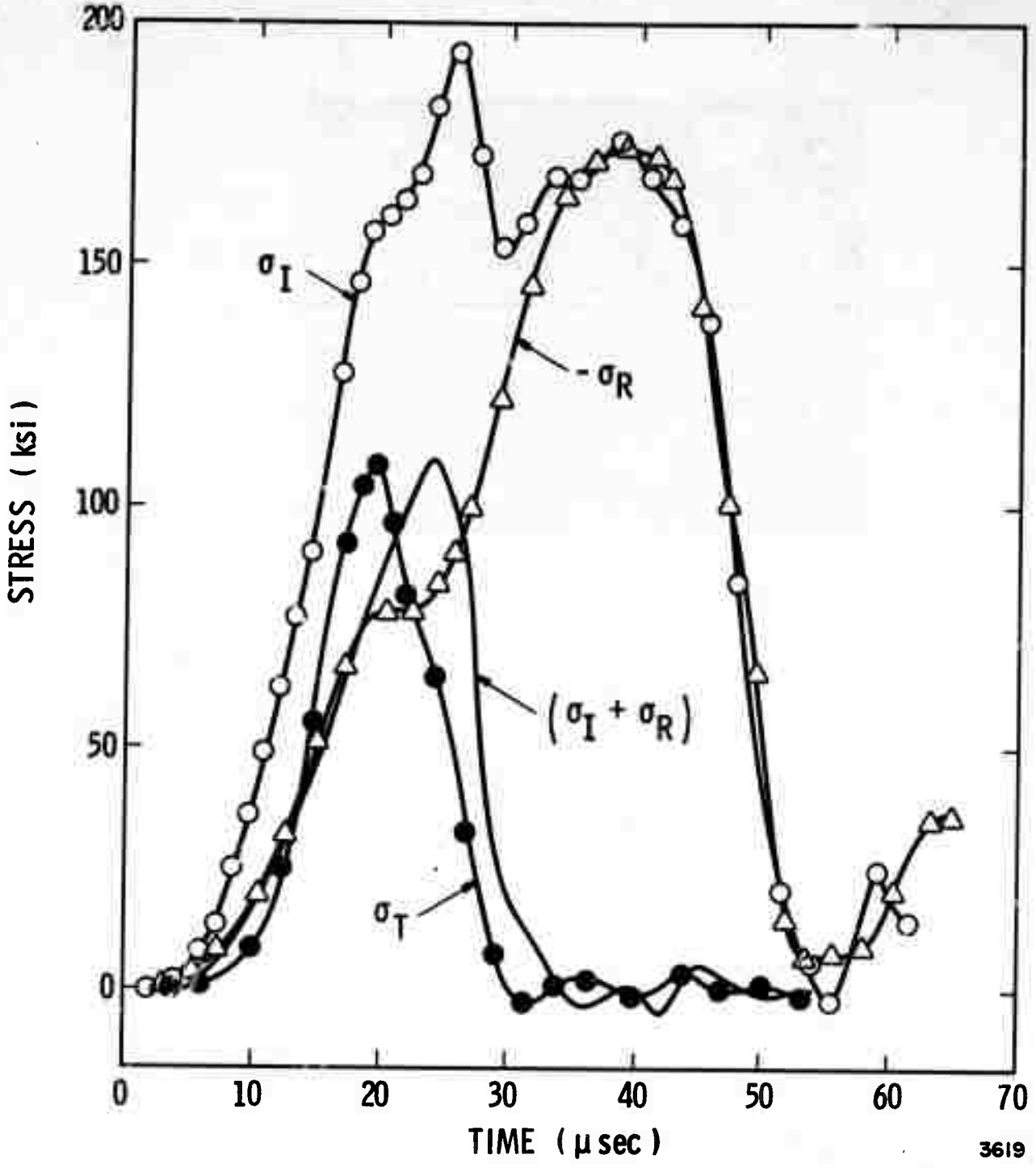

FIGURE 7. AMPLITUDE COMPARISON OF PULSES FROM PRESSURE BAR

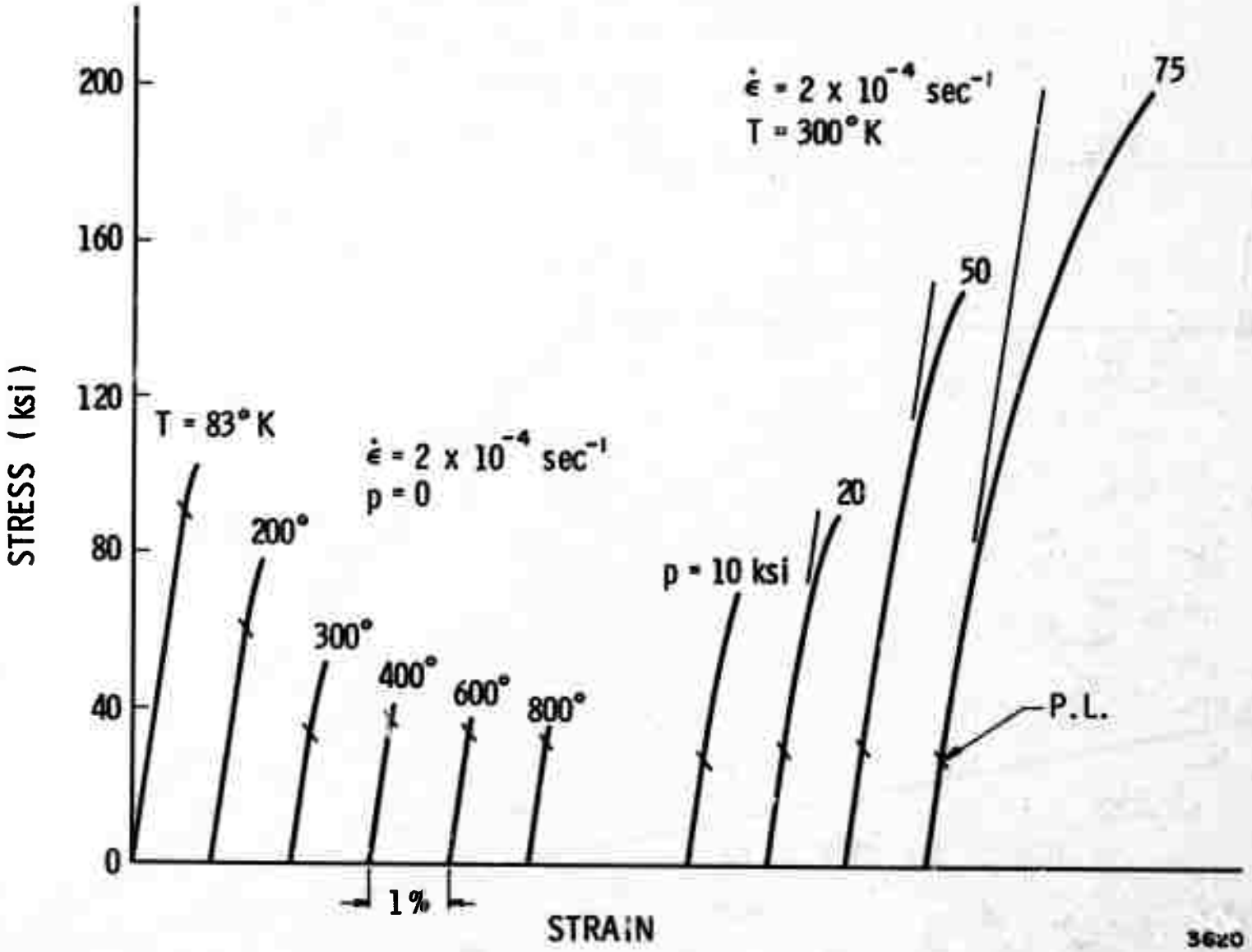

FIGURE 8. TYPICAL STRESS-STRAIN CURVES

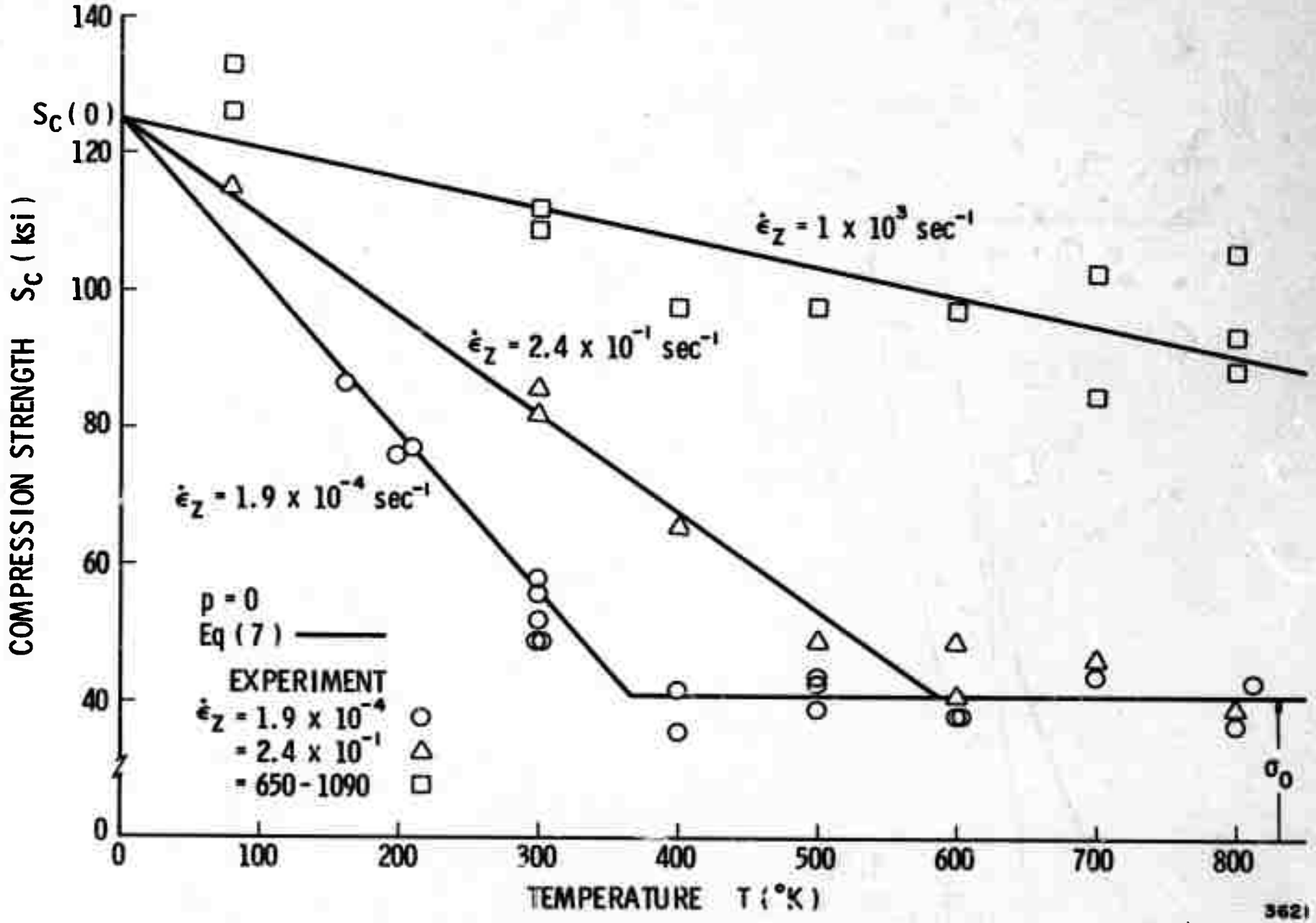

FIGURE 9. EFFECT OF TEMPERATURE AND STRAIN RATE ON UNCONFINED COMPRESSION STRENGTH

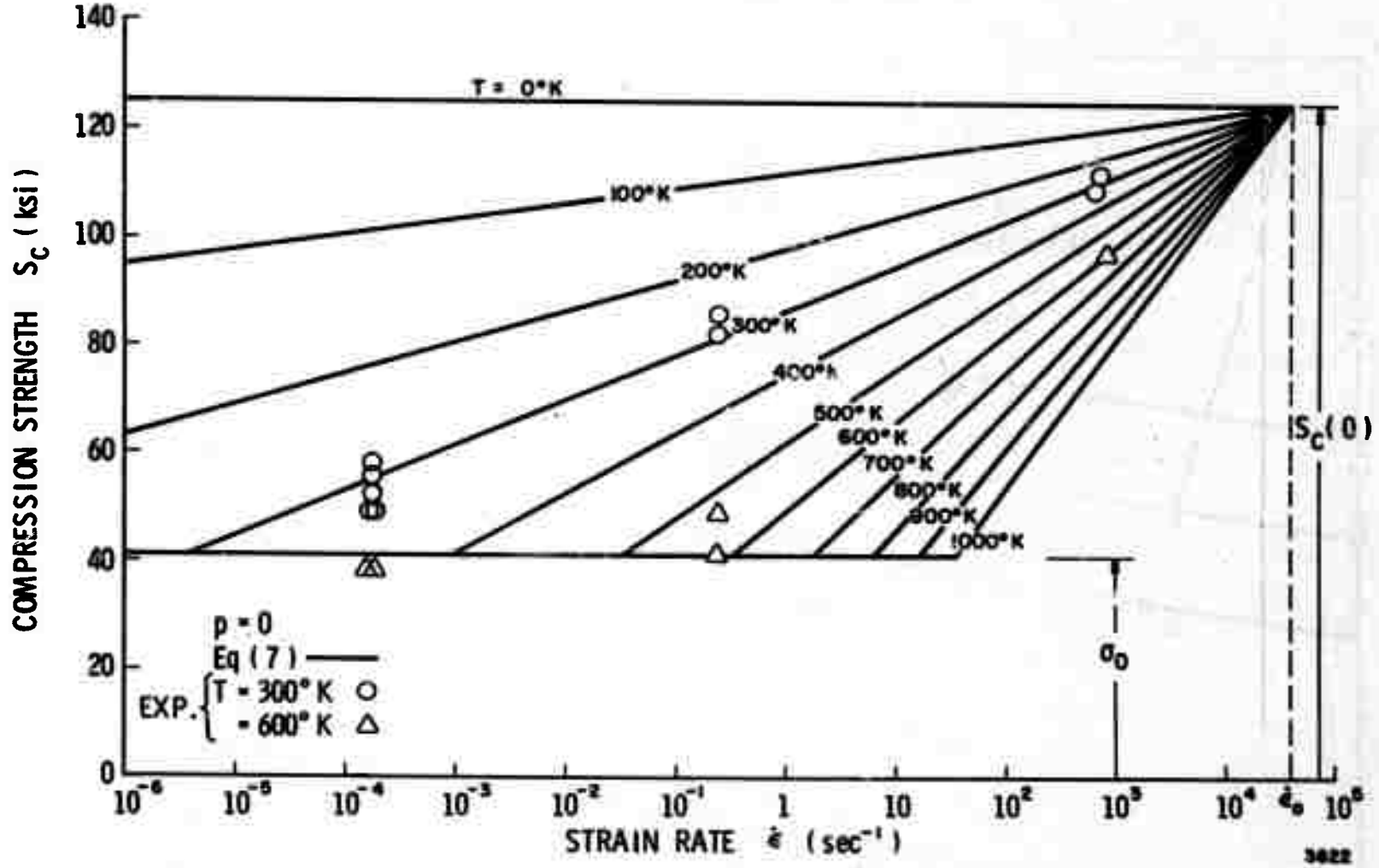

FIGURE 10. COMPRESSION STRENGTH PLOTTED AS A FUNCTION OF STRAIN RATE

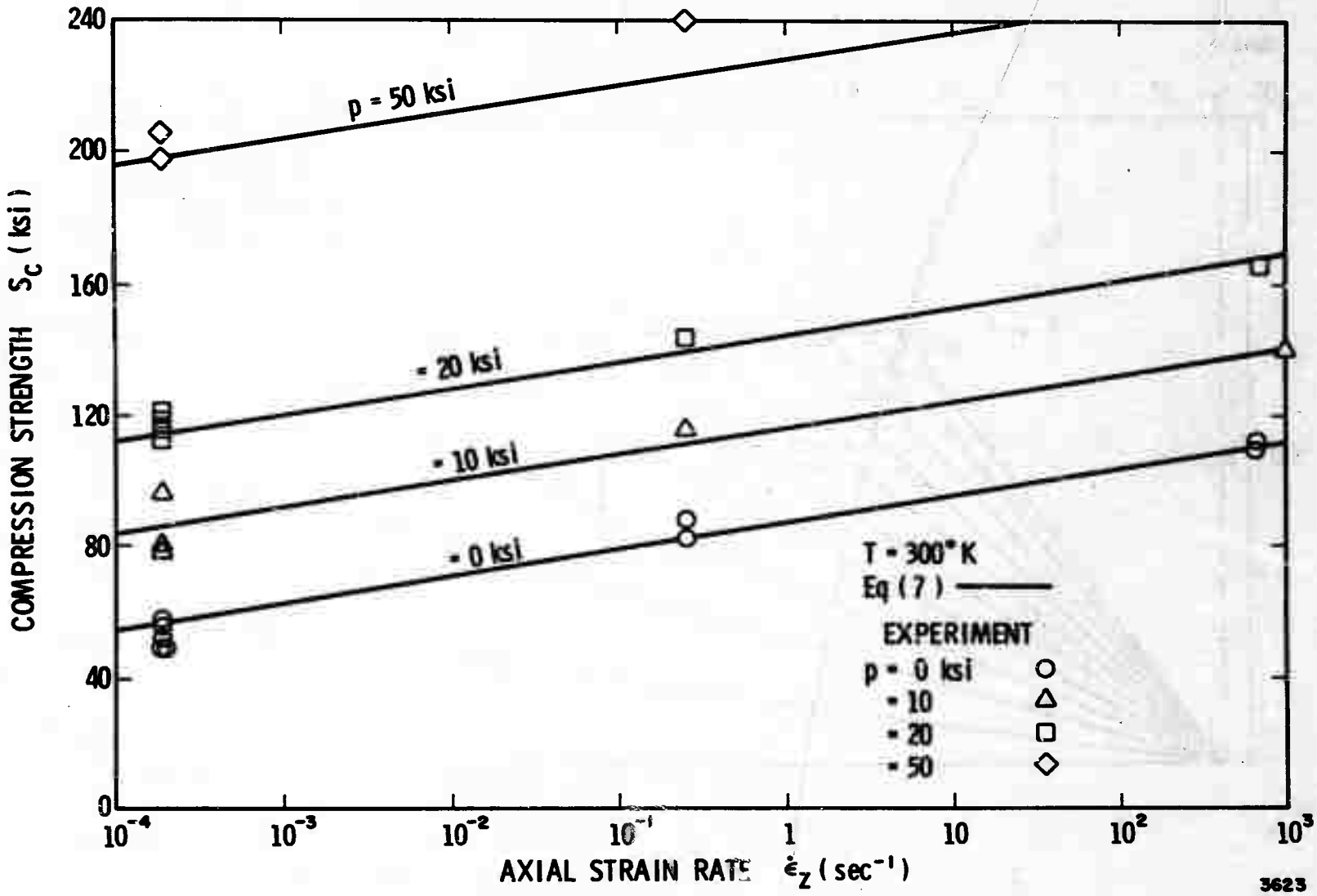

FIGURE 11. EFFECT OF CONFINING PRESSURE ON THE STRAIN-RATE DEPENDENCE OF THE COMPRESSION STRENGTH

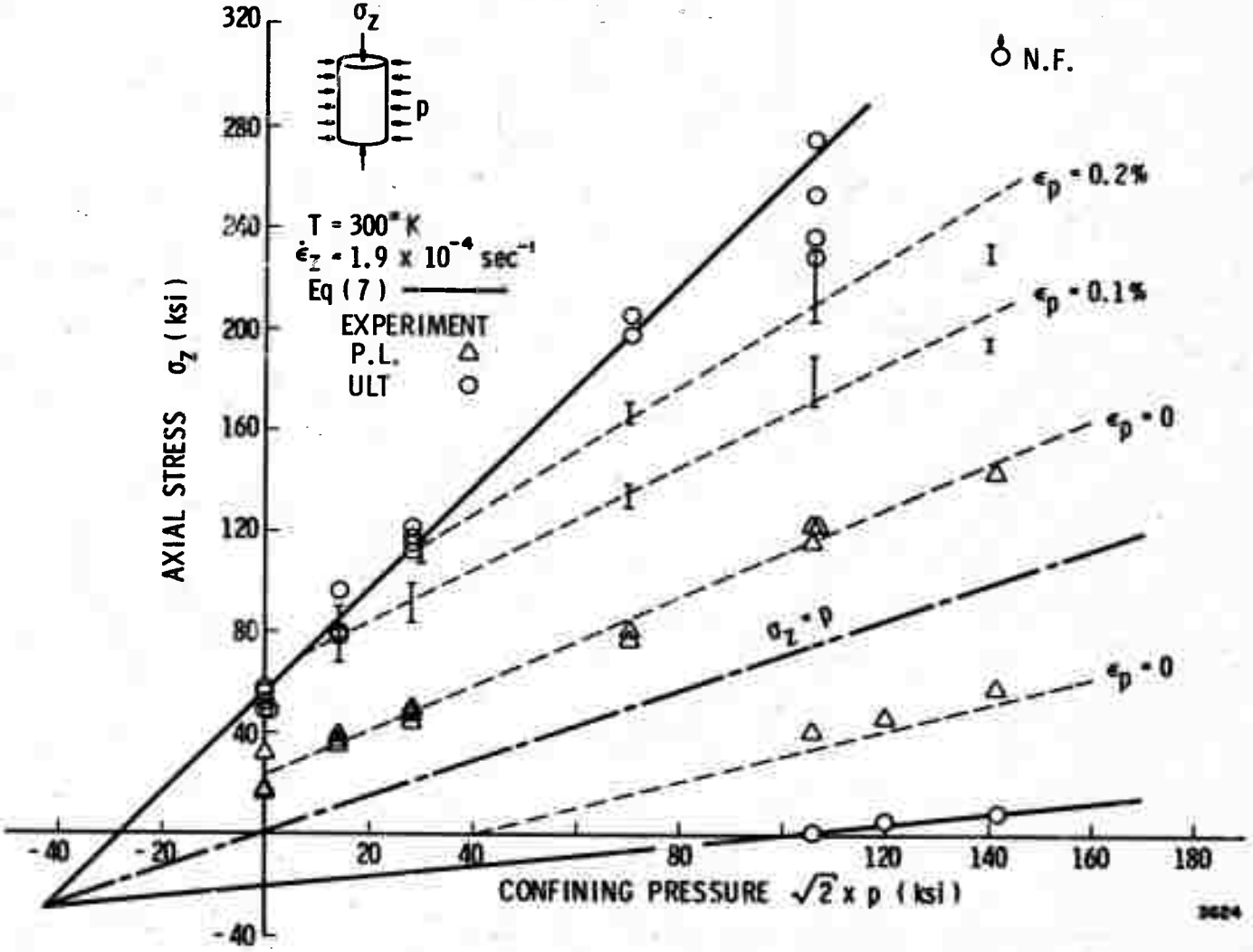

FIGURE 12. PLOT OF YIELD AND FRACTURE DATA IN THE PLANE OF THE HYDROSTATIC AND AXIAL STRESS AXES

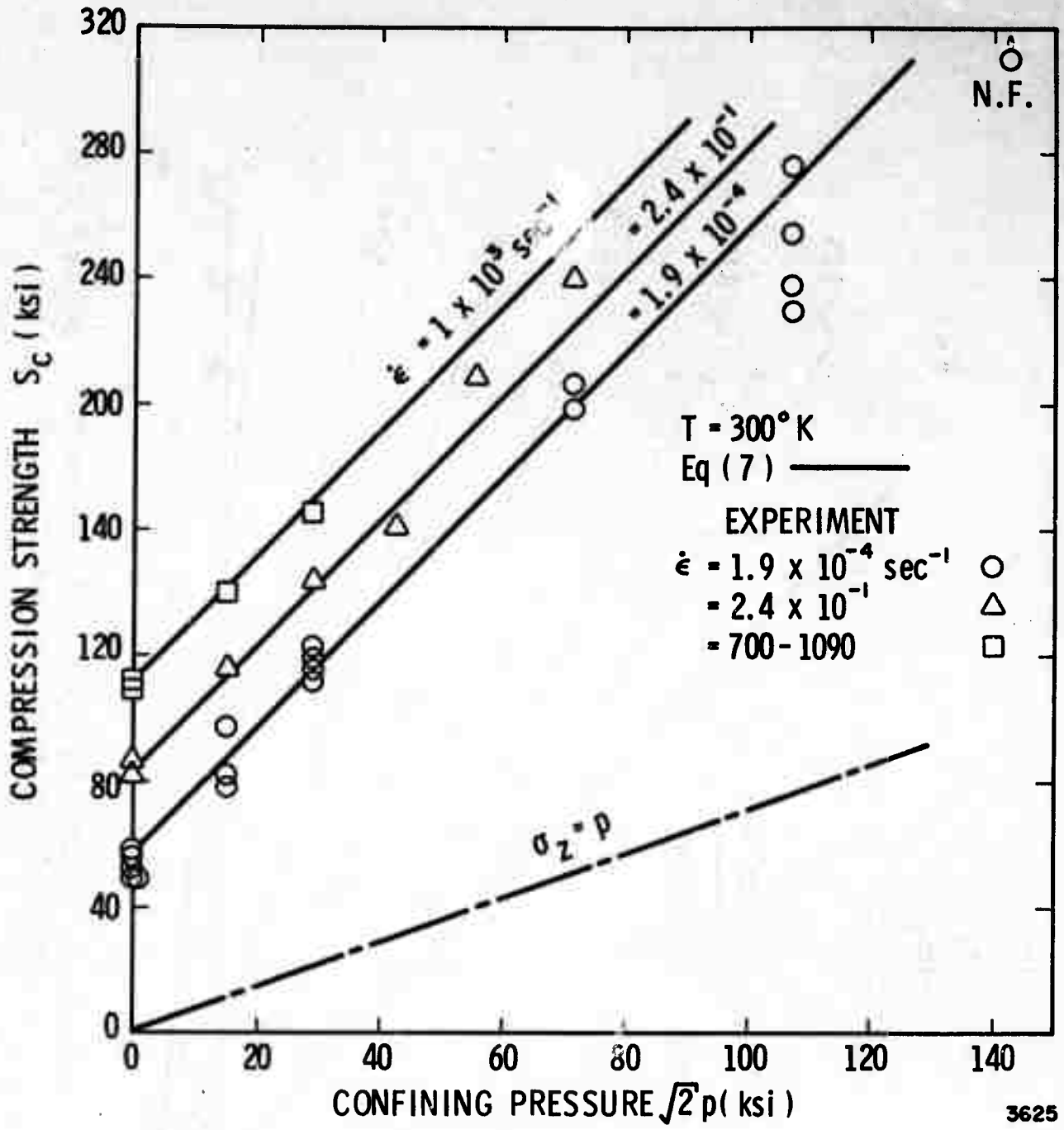

FIGURE 13. EFFECT OF STRAIN RATE AND PRESSURE ON THE COMPRESSION STRENGTH

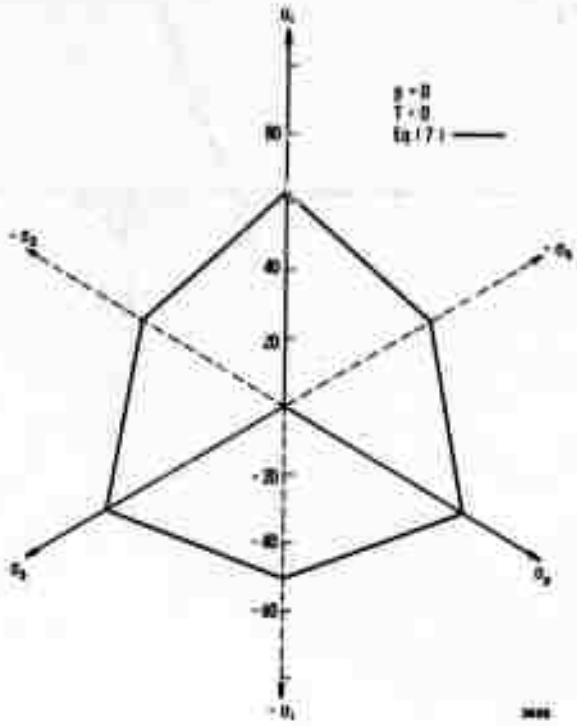

(a) The Deviatoric Plane

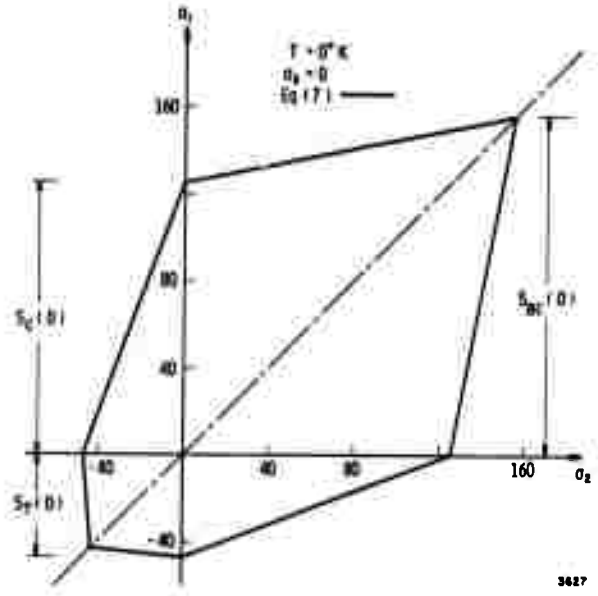

(b) The Biaxial Coordinate Plane

FIGURE 14. THE PREDICTED SHAPE OF THE FAILURE SURFACE FOR T = 0°K

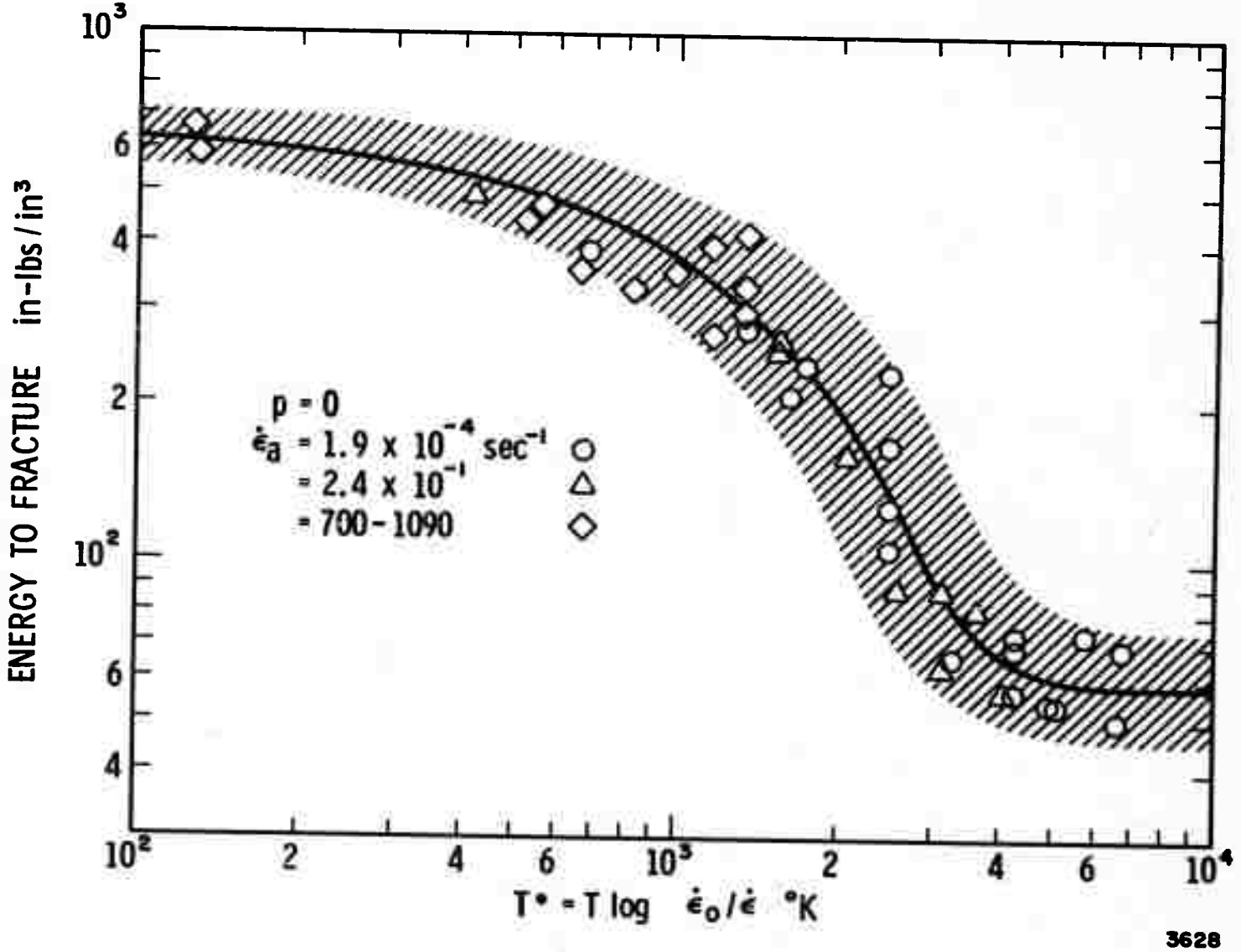

FIGURE 15. CORRELATION OF FRACTURE ENERGY FOR ALL UNCONFINED TESTS WITH A RATE-MODIFIED TEMPERATURE PARAMETER

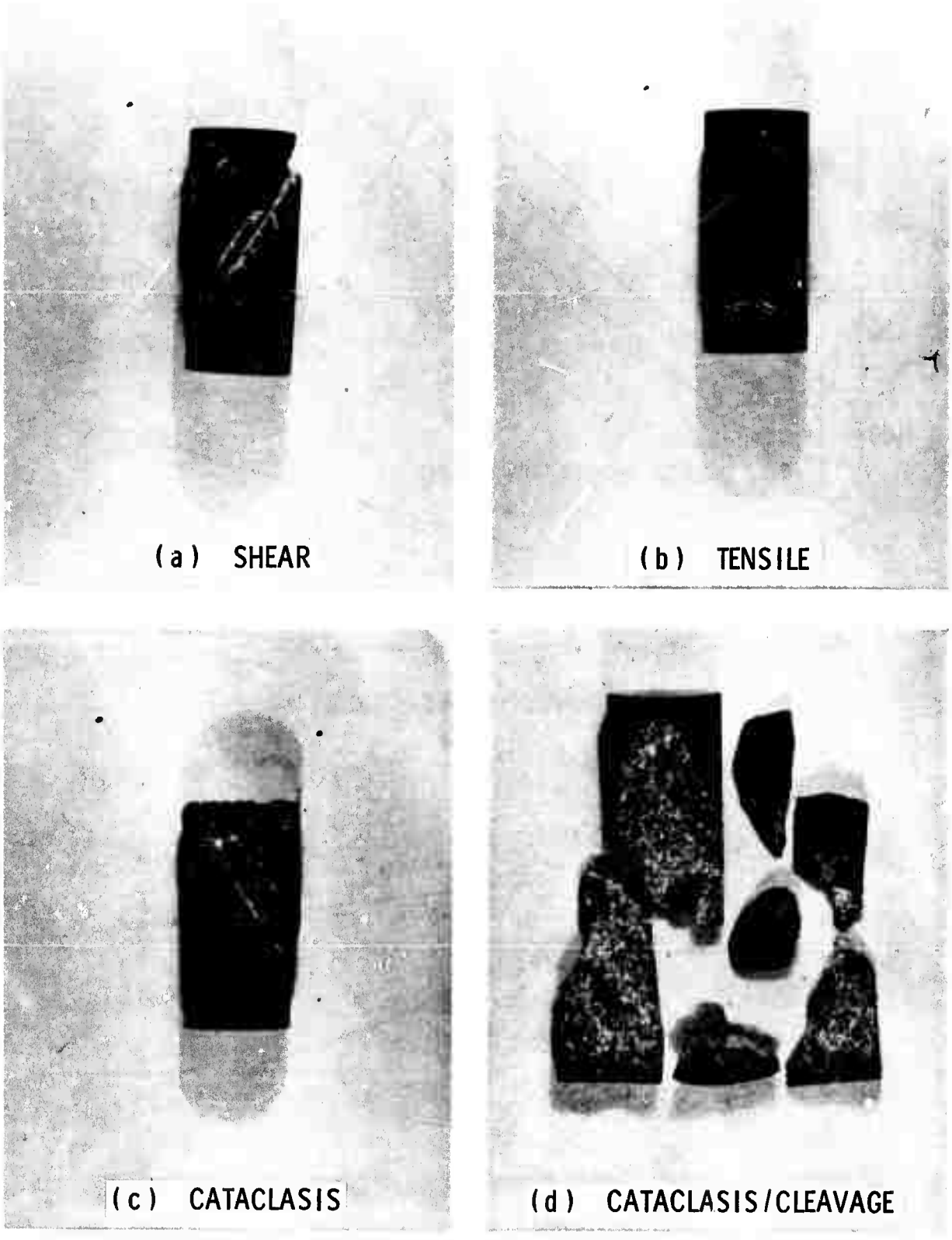

FIGURE 16. REPRESENTATIVE FAILURE MODES

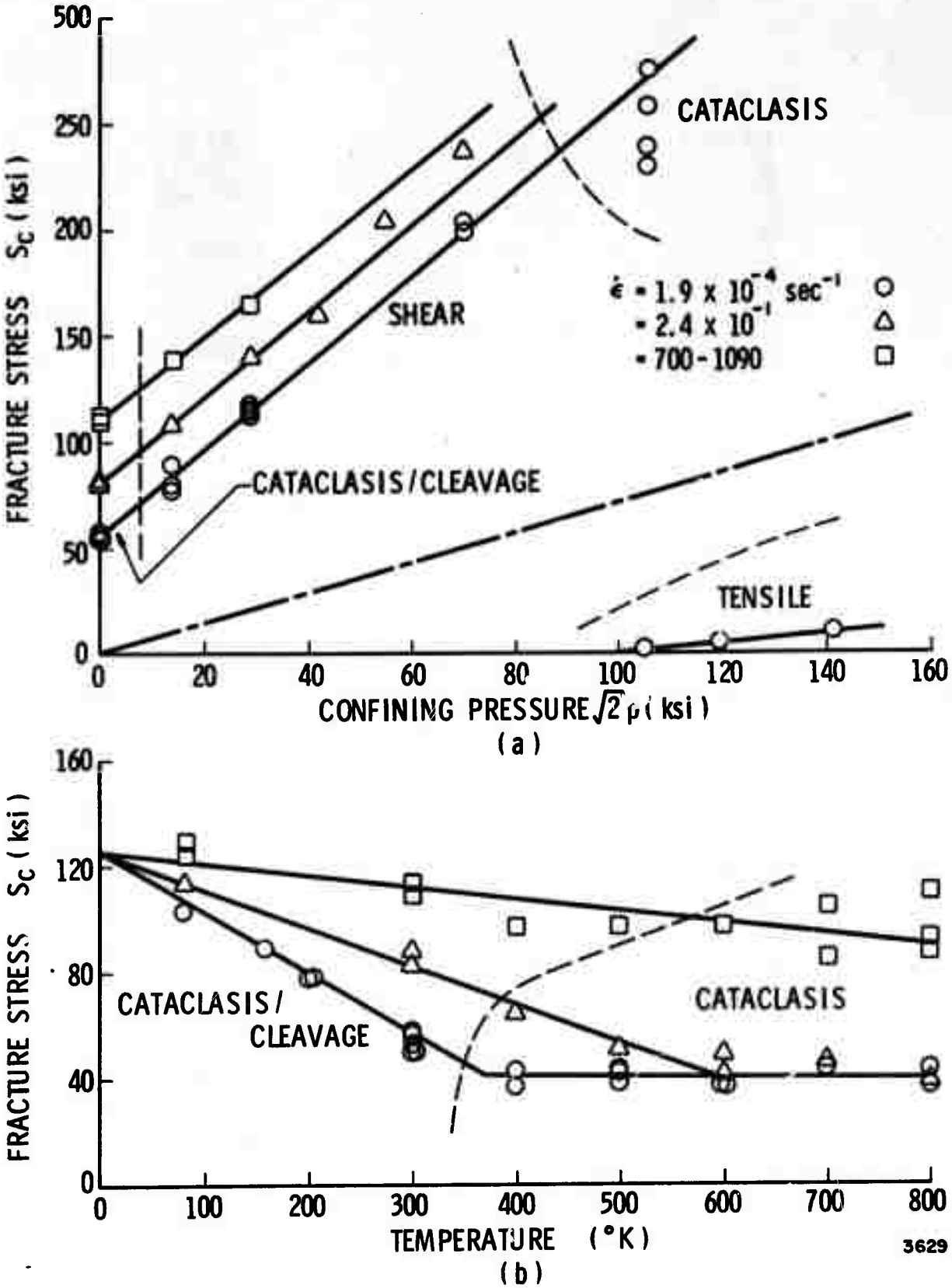

FIGURE 17. CORRELATION OF THE FRACTURE MODES WITH THE CONFINING PRESSURE